Realia et naturalia

DISSERTATIONES
CHIMICAE
UNIVERSITATIS
TARTUENSIS
126

KERLI TÕNURIST

Influence of electrospun separator materials properties on electrochemical performance of electrical double-layer capacitors

TARTU ÜLIKOOL · UNIVERSITAS TARTUENSIS · 1632

DISSERTATIONES CHIMICAE UNIVERSITATIS TARTUENSIS
126

DISSERTATIONES CHIMICAE UNIVERSITATIS TARTUENSIS
126

KERLI TÕNURIST

Influence of electrospun separator materials properties on electrochemical performance of electrical double-layer capacitors

UNIVERSITY OF TARTU
PRESS
1632

Institute of Chemistry, Faculty of Science and Technology, University of Tartu, Estonia

Dissertation is accepted for the commencement of the degree of Doctor of Philosophy in Chemistry on June 11th, 2013 by the Council of Institute of Chemistry, University of Tartu.

Supervisors: Prof. Enn Lust, University of Tartu, Estonia
Ph.D. Thomas Thomberg, University of Tartu, Estonia

Opponent: Prof. Thierry Brousse,
IMN (Université de Nantes-CNRS), France

Commencement: August 23rd, 2013, Ravila 14A (Chemicum), room 1021, 12.00

ISSN 1406–0299
ISBN 978–9949–32–331–9 (print)
ISBN 978–9949–32–332–6 (pdf)

University of Tartu Press
www.tyk.ee
Order No. 266

TABLE OF CONTENS

I. LIST OF ORIGINAL PUBLICATIONS

I. K. Tõnurist, A. Jänes, T. Thomberg, H. Kurig, E. Lust, Influence of mesoporous separator properties on the parameters of electrical double-layer capacitor single cells, J. Electrochem. Soc. 156 (2009) A334–A342.

II. K. Tõnurist, T. Thomberg, A. Jänes, I. Kink, E. Lust, Specific performance of electrical double layer capacitors based on different separator materials in room temperature ionic liquid, Electrochem. Commun. 22 (2012) 77–80.

III. K. Tõnurist, T. Thomberg, A. Jänes, T. Romann, V. Sammelselg, E. Lust, Influence of separator properties on electrochemical performance of electrical double-layer capacitors, J. Electroanal. Chem. 689 (2013) 8–20.

IV. K. Tõnurist, T. Thomberg, A. Jänes, E. Lust, Specific performance of supercapacitors at low temperatures based on different separator materials, J. Electrochem. Soc. 160 (2013) A449–A457.

V. K. Tõnurist, T. Thomberg, A. Jänes, E. Lust, Specific performance of electrical double-layer capacitors based on different separator materials and non-aqueous electrolytes, ECS Transactions 50 (43) (2013) 181–189.

VI. K. Tõnurist, T. Thomberg, A. Jänes, T. Romann, V. Sammelselg, E. Lust, Polymorphic behavior and morphology of electrospun poly(vinylidene fluoride) separator materials for non-aqueous electrolyte based electric double layer capacitors, ECS Transactions 50 (45) (2013) 49–58.

Author's contribution

Paper I: Performed all the electrospinning experiments and electrochemical measurements. Participated in the analysis of data and preparation of the manuscript.

Paper II: Performed all the electrospinning experiments, electrochemical measurements and analysis of data. Mainly responsible for the preparation of manuscript.

Paper III: Performed all the electrospinning experiments, electrochemical measurements and analysis of data. Mainly responsible for the preparation of manuscript.

Paper IV: Performed all the electrospinning experiments, electrochemical measurements and analysis of data. Mainly responsible for the preparation of manuscript.

Paper V: Performed all the electrospinning experiments, electrochemical measurements and analysis of data. Mainly responsible for the preparation of manuscript.

Paper VI: Performed all the electrospinning experiments, electrochemical measurements and analysis of data. Mainly responsible for the preparation of manuscript.

2. ABBREVIATIONS AND SYMBOLS

AN – acetonitrile
BET theory – Brunauer-Emmett-Teller theory
C – total capacitance
C' – real part of the capacitance
C'' – imaginary part of the capacitance
C_m – specific capacitance
C_p – parallel capacitance
C_s – series capacitance
CV – cyclic voltammetry
DMA – N,N-dimethylacetamide
DMF – N,N-dimethylformamide
DMC – dimethyl carbonate
E – electrode potential
EC – ethylene carbonate
EDLC – electrical double-layer capacitor
E_{max} – maximum specific energy
$EMImBF_4$ – 1-ethyl-3-methylimidazolium tetrafluoroborate
f – alternative current frequency
f_0 – characteristic relaxation frequency
I – current density
$I(j\omega)$ – current fasor
I_0 – initial current
$I(t)$ – output current
j – current
j – imaginary number
m – mass of one electrode
m_{tot} – mass of two electrodes
P – total porosity
p – pressure
p_0 – atmospheric pressure
p/p_0 – relative pressure
PC – propylene carbonate
P_{max} – maximum specific power
$P(\omega)$ – active power (i.e. real) component of the complex power

$Q(\omega)$ – reactive (i.e. imaginary) power component of the complex power
R – total resistance of the system
r – radius of the pore(s)
R_p – parallel resistance
R_s – series resistance
RTIL – room-temperature ionic liquid
S_{BET} – surface area, calculated using the Brunauer-Emmett-Teller theory
S_{Hg} – surface area, measured appling mercury intrusion porosimetry
S_{micro} – micropore surface area calculated using the *t*-plot method
$S(\omega)$ – complex power
T – temperature
t – time
$TEMABF_4$ – triethylmethylammonium tetrafluoroborate
TiC-CDC – TiC derived carbon
U – cell voltage
$U(j\omega)$ – voltage fasor
$U(t)$ – alternating voltage
U_0 – steady-state voltage
V_{micro} – micropore volume calculated using the *t*-plot method
V_{tot} – total pore volume
Z – impedance
Z' – real part of the impedance
Z'' – imaginary part of the impedance
$|Z(\omega)|$ – impedance modulus
v – voltage scan rate
θ – phase angle between voltage and current
θ_c – contact angle
τ_r – characteristic relaxation time
ω – angular frequency

3. INTRODUCTION

Electrospinning is a well-known method for processing the flexible and highly porous nanostructured (fibrous or porous layered) scaffolds by applying a high electric field strength to a droplet of polymer solution or melt [1–22]. By varying different electrospinning parameters the fiber diameter, porosity and membrane morphology can be easily influenced. Due to the good flexibility, high porosity and easily influenced morphology, electrospun nanofiber membranes have very wide-ranging technological applications [4–9,11,21], starting from medicine and nanosensors and finishing with the energy storage devices. It has been demonstrated that the electrospun nanofiber mats can be used as a separator material in the electrical double-layer capacitor (EDLC) [23–28].

EDLCs, also known as supercapacitors and ultracapsacitors, are energy storage devices with short charging and discharging times and high electrical efficiency (up to 98%), power density and very good cyclability (rechargeable over 10^6 cycles) [29–38]. During last 15 years intensive research work has been done to improve the energy and power densities and cyclability of EDLC, designing the various porous electrode materials and electrolytes applicable for high energy and power density EDLCs.

However, little attention has been given for the role of separator material and its influence on the electrochemical performance of EDLCs. The properties of the separator material used in EDLC are important as they give a significant contribution to the overall series resistance of a cell. Separator has an important effect on the ionic charge compensation rate between positively and negatively charged microporous carbon electrodes soaked into the non-aqueous electrolyte solution. Therefore the molar conductivity of ions in the porous separator matrix is extremely important [23–28].

The main aim of this work was to study the influence of the separator material characteristics (chemical composition, surface morphology, total porosity, specific surface area, pore size distribution and thickness) on the performance of EDLC, including energy and power densities, and the characteristic relaxation time.

4. LITERATURE OVERVIEW

4.1. Electrospinning method

Electrospinning is a process where a high *dc* voltage is used to create an electrically charged jet of polymer solution or melt. This process was patented in 1934 by Formhals [1], wherein an experimental setup was outlined for the production of polymer filaments using electrostatic force. Electrospinning apparatus presented in Figure 1, consists of three main components: a high voltage supplier, a capillary tube with a needle and a metal collecting screen (collector), which is grounded [4,5,7,8,22]. One electrode is placed into the spinning solution and the other attached to the collector. Electric field is subjected to the end of a capillary tube and the grounded collector plate. When charges within the fluid reached a critical amount, a fluid jet will erupt from the droplet at the tip of the needle to form a conical shape polymer solution jet known as the Taylor cone. With increasing electric field strength, the electrostatic force overcomes the surface tension and a charged jet of fluid is ejected from the tip of the Taylor cone. The charged polymer solution jet undergoes a whipping process wherein the solvent evaporates, leaving behind a charged polymer fiber, which is deposited randomly on a collecting screen [4,5,8].

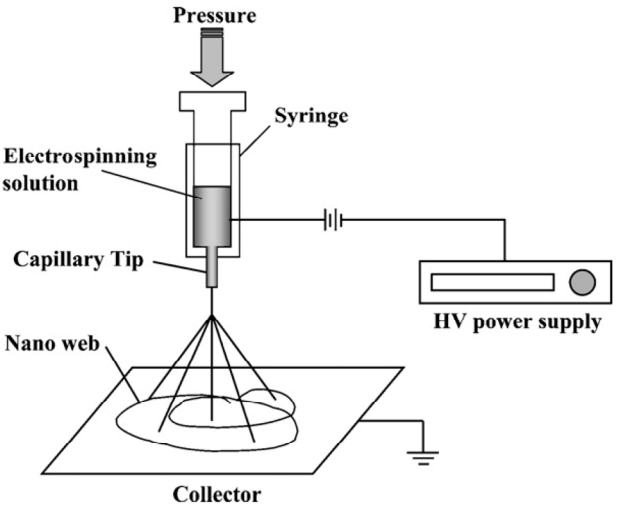

Figure 1. Electrospinning setup [22].

4.1.1. Electrospinning process

The electrospinning process can be influenced by various parameters and thereby influence the morphology and properties of the final membrane [4–13,21]. These parameters may be broadly classified into three main groups: polymer solution characterising parameters, processing conditions, and ambient conditions [4,7,8]. The most important polymer solution parameters are the molecular weight of a polymer (must be high enough for entanglement), the solution concentration (determines the viscosity of a polymer solution), and the chemical composition of the solvent used (its dielectric constant, volatility, boiling point). The processing conditions include the *dc* voltage (i.e. the electric field strength), polymer solution feed rate, inner diameter of the needle, distance from the needle tip to the collector plate and type of the collector. Ambient conditions as humidity and chemical composition of the atmosphere may also have some effect on the electrospun fiber morphology and surface composition [4,5].

4.1.1.1. Polymer solution parameters

The properties of the polymer solution have the most significant influence on the electrospinning process and on the resultant fiber morphology [4]. For electrospinning to occur solution must consist of polymer of sufficient molecular weight and the solution must be of sufficient viscosity. For maintaining the continuity of the jet during electrospinning, a good entanglement of the molecule chain within the solution is needed. The polymer chain entanglements were found to have a significant impact on whether the electrospinning jet breaks up into small droplets or whether the resultant electrospun fibers contain beads [4,7,13].

At lower viscosity, the higher amount of solvent molecules and fewer chain entanglements will mean that the surface tension has a dominant influence along the electrospinning jet causing beads to form along the fiber. Surface tension has the effect to decrease the surface area per unit mass of a fluid. When the viscosity increases, there is a gradual change in the shape of the beads from spherical to spindle-like until smooth fiber is obtained. It has been found that with increased viscosity, the diameter of the fibre also increases, probably due to the greater resistance of the solution to be stretched by the charges on the jet [4,7,10,11,16].

Stretching of the electrospinning jet is caused by repulsion of the charges at its surface. Therefore, the amount of charges that can be carried by the electrospinning jet depends on the conductivity of the polymer solution. Solutions prepared using solvents of higher conductivity generally yield fibers without beads, while no fibers are formed, if the solution has zero conductivity [4,5,14].

Solvents with different dielectric constant values will interact very differently with the electrospinning field and it is therefore an important material parameter in the electrospinning process. For solution of high dielectric constant, the surface charge density on the jet tends to be more evenly dispersed. Therefore, solvents having higher dielectric constant produce fibers with smaller diameter [4,14,15].

Invariably, it is the evaporation of solvent from the jet that yields to formation of a solid polymer fiber at the collector plate. Ideally, all traces of a solvent must be removed by the time the fiber reaches the collector. If not, the wet fibers may fuse together to form a melted or reticular mat [4,5,16,21].

4.1.1.2. Processing conditions

Various external factors can affect the electrospinning process – this include the *dc* voltage supplied, the polymer solution feed rate, diameter of the needle, distance between the needle tip and collector, and the type of collector. These parameters have a certain influence on the fiber morphology, although they are less significant than the solution parameters [4–13].

A crucial element in electrospinning is the application of a high *dc* voltage to the solution. The high voltage will induce the necessary charges on the solution and, together with the external electric field, will initiate the electrospinning process when the electrostatic force in the solution overcomes the surface tension of the solution. As both the *dc* voltage supplied and the resultant electric field have an influence on the stretching and acceleration of the jet, they will have an influence on the morphology of the fibers obtained [4,5,7].

The polymer solution feed rate will determine the amount of solution available for electrospinning. There is a corresponding feed rate for a given *dc* voltage if a stable Taylor cone is to be maintained. When the polymer solution feed rate is increased, there is a corresponding increase in the fiber diameter or beads size, as there is a greater volume of solution that is drawn from the needle tip into the electric field [4,11,16,21].

The internal diameter of the needle or the pipette orifice has an effect on the size of electrospun fibers. A smaller internal diameter of needle has been found to reduce the fiber diameter as well as the amount of beads on the electrospun fibers [4,5,17].

Variation of the distance between the tip and the collector will have a direct influence on both the flight time and the electric field strength. For individual fibers to form, the electrospinning time must be optimal for most of the solvents to be evaporated. When the distance between the tip and the collector is reduced, the jet will have a shorter distance to travel before it reaches the collector. When the distance is too low, excess solvent in deposited fibers may cause the fibers to merge, where they contact to form junctions resulting in inter and intra layer bonding [4,11,18].

The simplest and the most used collector, reported for laboratory-scale electrospinning, is a stationary metal plate or a foil placed at a fixed distance from the tip [4,5,8]. Rotating drum allows more evenly deposited fibers and some degree of velocity-dependent alignment of fibers [4,5,7,8,11,12,19].

4.1.1.3. Ambient parameters

Effect of the electrospinning jet surrounding parameters is one area which is still poorly investigated. Any interaction between the surrounding and the polymer solution may have an effect on the electrospun fiber morphology [4].

It has been found that high humidity may cause the formation of pores on the surface of the fibers. The humidity of environment will also determine the rate of evaporation of the solvent from solution. At a very low humidity, a volatile solvent may dry very rapidly. The needle tip may clog when the evaporation of the solvent is faster than the removal of the solution from the tip of the needle [4].

The chemical composition of air in the electrospinning environment will have an effect on the electrospinning process. Different gases have different behaviour under high electrostatic *dc* field [4].

4.1.2. Characterisation of nanofibers and membranes

Electrospun polymer nanofibers in the form of membrane have many potential applications in the field of biotechnology, environmental engineering, electronics and energy technology [4–9,11]. The morphology of single fiber as average diameter, pores on the fiber surface as well as the morphology of nanofibrious membrane, such as total porosity and surface area, are basic properties of the deposited nanofibers. Morphology of the electrospun polymer nanofibers can be characterised by scanning electron microscopy (SEM) method, after the sample surface is covered with thin layer of conducting material. Pores play an important role in determining the physical and chemical properties of the porous membrane and have a deterministic effect on the performance of filters, catalysts, adsorbents, etc. [4–9]. To design electrospun membranes for a specific application it is necessary to analyse the pore-size distribution, total specific surface-area and porosity of the membrane. Two types of pores can be identified: pores on/within each fiber and pores (empty spaces) between the fibers. Pore sizes can be measured using direct (SEM, TEM) or indirect (bubble point measurement, mercury intrusion porosimetry) methods [4].

4.1.2.1. Mercury intrusion porosimetry

The porosity of a material can be measured using mercury intrusion porosimetry method. In this technique, a nonwetting liquid (usually mercury), that does not dissolve or swell the nanofibers, is compressed into the porous membrane. Forcing mercury into the pores of the material requires the application of a pressure p to the mercury column in contact with the sample. As p is gradually raised, increasingly smaller pores in the porous material are intruded by the mercury [5,39–41]. The relationship between the applied pressure p and the pore radius r accessed by Hg is given by the Washburn equation [42]:

$$r = -2\gamma \cos\theta_c / p \,, \tag{1}$$

where θ_c is the contact angle (141.3° for mercury) and γ is the surface tension (484 mN m^{-1} for mercury) of the liquid. This technique measures only the fraction of porosity accessible by the mercury atoms and therefore excludes closed pores as well as small mesopores (r < 3–4 nm) that are inaccessible by mercury. Very large pores (hundreds of micrometers in size) are readily flooded by mercury even before application of pressure to initiate the intrusion of Hg [5,39].

4.2. Electrical double-layer capacitors

Electrical double-layer capacitors (EDLCs) store the energy in electric field of the electrochemical double-layer formed at a solid|electrolyte interface (Fig. 2). Thickness of the double-layer depends on concentration of the electrolyte and on the effective size of the ions and is in the order of 5–10 Å for concentrated electrolytes. Positive and negative ionic charges within the electrolyte accumulate at the surface of the solid electrode and compensate the electronic charge at the electrode surface [30]. EDLCs are able to store and deliver energy at relatively high rates because the charges are mainly stored through physical adsorption processes of ions and there is no electron transfer (faradic processes) through the electrode|electrolyte interface. This enables EDLCs to have very high power but moderate energy densities and high degree of cyclability, usually over 100,000 cycles [29–31,33,37,38].

A high internal resistance limits the power capability of the capacitor and ultimately its application. In EDLCs a number of sources contribute to the internal resistance and are collectively measured and referred to as the equivalent series resistance. These are resistance of the electrode material, the interfacial resistance between the electrode and the current collector, the ionic resistance of ions moving in small pores, the ionic resistance of ions moving through the separator, and the electrolyte resistance [29–31,43].

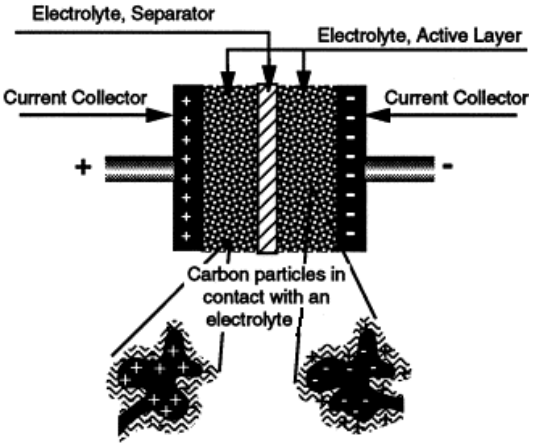

Figure 2. Scheme of EDLC cell [30].

4.2.1. Carbon as an electrode material for EDLCs

The attraction of porous carbon as an EDLC electrode material arises from an unique combination of chemical and physical properties, like high conductivity, high surface-area (up to 2500 m^2 g^{-1}), good corrosion resistance, high temperature stability, controlled pore structure, processability and compatibility in composite materials and relatively low cost [29–31,33,38,44,45]. The majority of carbon materials are derived from carbon-rich organic precursors by heat treatment in inert atmospheres. Natural materials, such as coconut shells, wood, pitch, coal or synthetic materials, such as nanowire polymers, polymer aerogels, can be used as precursors [37,38,46–52]. The capacitance of a device is largely dependent on the characteristics of the electrode material. The electrical properties of carbon materials are directly related to their structure, determined mainly by the ratio of σ, sp^3 and sp^2 bonded carbon structure. It is usually anticipated that the capacitance of a porous carbon will be proportional to its available surface area, but in practice, it usually represents an oversimplification [31,37,38]. The major factors that contribute to the complex relationship are: (i) assumptions in the measurement and the applicability of the electrode surface area; (ii) variations in the specific capacitance of carbons with different morphology; (iii) variations in surface chemistry; (iv) variations in the conditions under which the carbon capacitance is measured [31].

The double-layer capacitance of activated carbon varies from 100 to 130 F g^{-1} in organic electrolytes and this value can exceed 150–300 F g^{-1} in aqueous electrolytes. However, at noticeably lower cell voltage can be applied in the case of aqueous electrolytes because the electrolyte voltage stability is limited by the water decomposition process [29,31,37,44,45].

4.2.2. Role of separator materials in EDLCs

Separator in EDLC separates the negatively and positively charged electrodes from each other and has an effect on the ionic charge compensation rate between the positively and negatively charged microporous carbon electrodes soaked into the electrolyte solution. Therefore, the molar conductivity of ions in the porous separator matrix is extremely important [23–28]. Generally, porous polymer membranes or fibrous materials are used for this purpose. Separator material must not conduct electrons, and has to be chemically and electrochemically stable towards the electrolyte and electrode material. A low thickness is required for high energy and power density EDLC, and an appropriate porosity and pore size is necessary to hold sufficient liquid electrolyte for the ionic conductivity between the electrodes. The separator should wet easily in the electrolyte, but remain its mechanical strength and dimensional stability [53].

4.2.3. Electrolytes in EDLCs

Both aqueous and non-aqueous electrolytes, and room-temperature ionic liquids are used in EDLCs. The electrolyte should be resistant to electrochemical reduction and oxidation at carbon electrode and produce high specific capacity at the carbon|electrolyte interface. The electrochemical stability of an aqueous electrolyte is limited by the thermodynamic stability limit of water, corrected by the faradic reaction activation overpotential. Accordingly, the larger the electrolyte stability voltage region, the higher the EDLC cell voltage can be applied [33]. Consequently, in aqueous electrolytes the voltage region is up to 1.23 V, but in non-aqueous electrolytes up to 3.2 V, and in ionic liquids even up to 3.5 V [23–26,29,54–56]. Ionic liquids are room-temperature liquid solvent free electrolytes and their voltage region is driven by the electrochemical stability of the ions. The main requirements for suitable non-aqueous electrolytes are following [29]:

i. Wide region of electrochemical stability (i.e., the high decomposition over voltage of the solution). This region should be somewhat larger than the intended operating range of the EDLC in order to minimize problems arising from adventitious overcharge.
ii. Minimum viscosity of the electrolyte in order to maximize the ionic mobility and resulting conductivity.
iii. Maximum solubility of the salt in the electrolyte to maximize the molar conductivity.
iv. Minimum ion pairing at given practical electrolyte concentration, to maximize the conductivity.
v. Optimal dielectric permittivity or donor number of the electrolyte to maximize the salt solubility and minimize the ion pairing.

Usually the solvents favoured for EDLCs are aprotic ones, i.e. not containing electrochemically active H atoms, to avoid cathodic evolution of H_2 from active protons in the structure of the solvent [29].

4.3. Electrochemical measurement techniques and interpretation of data

4.3.1. Cyclic voltammetry

Cyclic voltammetry (CV) is an electrochemical technique where the potential of system studied is changed linearly with time. The voltage scan rate, v, can be varied from a few millivolts per second to hundred volts per second. In this method the electrode potential is linearly varied from an initial (E_1) to final (E_2) potential and then swept back at the same scan rate to initial (E_1) potential. CV method is very useful to characterise the nature and reactivity of the products formed in an electrochemical reaction. The processes taking place between the electrode surface and electrolyte can proceed through two different ways, which are faradic and non-faradic processes. Faradic processes are arising from electron transfer across the electrode|electrolyte interface and it causes a current (j) peak to occur in the cyclic voltammogram. Non-faradic processes take place when the adsorption and desorption of ions from the electrode surface result in an electric current due to charging of the double-layer. When non-faradic adsorption process occurs on the electrode surface, no current peaks are observed and current measured can be associated with the electrical double-layer charging known as an ideal capacitive behaviour of an electrochemical system [29,44].

In the case of two-electrode system, the value of capacitance C can be calculated from I, U curve according to Eq. (2)

$$C = I(dU/dt)^{-1}, \tag{2}$$

where U is the cell voltage difference between the two oppositely charged electrodes, I is the current density and t is the time [23–27,57–60]. Equation (2) can be used to calculate the capacitance value only in the case of slow voltage scan rate, if the value of current is very small, as the ohmic potential drop (IR-drop) is negligible only under these conditions, and the current response is essentially equal to that of a pure capacitor [29]. At these conditions assuming to the first approximation that the capacitance of both electrodes is equal, the specific capacitance C_m (F g^{-1}) can be obtained from the capacitance of the cell by the Eq. (3)

$$C_{\mathrm{m}} = \frac{2C}{m}, \tag{3}$$

where m is the mass (g) of one electrode [23–27,57–60].

4.3.2. Electrochemical impedance spectroscopy

Electrical measurements to evaluate the electrochemical behavior of the electrode and/or electrolyte materials in EDLCs are usually performed with test cells completed with two identical electrodes. The general approach is to apply an electrical stimulus (a known voltage or current) to the electrodes and observe the electrochemical response (the resulting current or voltage). It is assumed that the properties of an electrode|electrolyte|separator system are time-invariant, and one of the basic purposes of electrochemical impedance spectroscopy is to determine these properties, their interrelations, and their dependencies on such controllable variables as temperature, applied direct voltage or current bias, etc. [61]. Some processes are taking place throughout the test cell, when it is electrically stimulated, mainly associated with the transport of electrons through the electronic conductors, charge transfer on electrode|electrolyte interface, and/or transport of ions through electrolyte and separator. The flow rate of charged particles through the interface (i.e. current density) depends on the ohmic resistance of the electrodes, separator, and the electrolyte as well as on the faradic reactions rates at the electrode|electrolyte interfaces. The total current depends on the electrical double-layer charging current, mass transfer rate, faradic reaction rate on the electrode|electrolyte interface, and on the series resistance of the electrodes, electrolyte and wetted separator used [24–26,61,62].

The impedance of an electrochemical system is measured by applying a low amplitude alternating voltage $U(t)$ to a steady-state voltage U_0, with

$$U(t) = U_0 \sin(\omega t), \tag{4}$$

where $\omega=1/(2\pi f)$ is the angular frequency, f is the *ac* frequency and t is the time. In a linear electrochemical system, the response signal $I(t)$ is shifted in phase θ (phase difference between voltage and current) and $I(t)$ has a different amplitude I_0:

$$I(t) = I_0 \sin(\omega t + \theta). \tag{5}$$

To simplify calculations, equations (4) and (5) can be rewritten in following forms:

$$I = I_0 e^{j\theta} e^{j\omega t} = I(j\omega) e^{j\omega t}, \tag{6}$$

$$U = U_0 e^{j\theta} e^{j\omega t} = U(j\omega) e^{j\omega t} = RI(j\omega) e^{j\omega t} + \frac{1}{C} \frac{I(j\omega) e^{j\omega t}}{j\omega}, \tag{7}$$

where $j \equiv \sqrt{-1}$, C is the total capacitance, R is the total resistance and $I(j\omega)$ and $U(j\omega)$ are the current and voltage fasors arising from the phase angle, respectively. The electrochemical impedance (complex resistance), $Z(\omega)$, is defined as:

$$Z(\omega) = \frac{U(j\omega)}{I(j\omega)} = R(\omega) + \frac{1}{j\omega C(\omega)} = Z' + jZ'', \tag{8}$$

where Z' and Z'' are the real part and the imaginary part of the impedance, respectively, defined as $Z'^2 + Z''^2 = |Z(\omega)|^2$; C is the total capacitance, R is the total resistance [34,61].

Using the resistive-capacitive circuit, usually observed for electrochemical systems, the series resistance, R_s, series capacitance, C_s, parallel resistance, R_p, and parallel capacitance, C_p, can be calculated from the impedance data [54,61]:

$$R_s = Z'(\omega), \tag{9}$$

$$C_s = -\frac{1}{\omega Z''(\omega)}, \tag{10}$$

$$R_p = R_s \left(1 + \frac{1}{\tan^2\left(\frac{Z'(\omega)}{Z''(\omega)} \right)} \right), \tag{11}$$

$$C_p = C_s \left(1 + \tan^2\left(\frac{Z'(\omega)}{Z''(\omega)} \right) \right). \tag{12}$$

4.3.3. Calculation of complex power and characteristic relaxation time constant

The values of the real part $C'(\omega)$ and imaginary part $C''(\omega)$ of capacitance can be calculated according to following equations:

$$C_s(\omega) = C'(\omega) - jC''(\omega), \tag{13}$$

$$C'(\omega) = -\frac{Z''(\omega)}{\omega|Z(\omega)|^2};\ C''(\omega) = \frac{Z'(\omega)}{\omega|Z(\omega)|^2}, \tag{14}$$

where $|Z(\omega)|$ is the impedance modulus. It should be noted that the low frequency part of $C'(\omega)$ for the EDLC cell corresponds to the so called static capacitance, which is measured during the constant current discharge, and $C''(\omega)$ corresponds to the energy dissipation by an irreversible faradaic charge transfer process, which can lead to the hysteresis of the electrochemical processes [23,25,43,54].

The values of complex power can be expressed as

$$S(\omega) = P(\omega) + jQ(\omega), \tag{15}$$

where the real part of power

$$P(\omega) = \omega C''(\omega)\left|\Delta U_{rms}\right|^2, \tag{16}$$

and the imaginary part of power

$$Q(\omega) = -\omega C'(\omega)\left|\Delta U_{rms}\right|^2, \tag{17}$$

with $\left|\Delta U_{rms}\right|^2 = \Delta U_{max}/\sqrt{2}$ (U_{max} is the maximal amplitude of ac voltage) [23,25–27,34,54,57,59].

System with the ideal capacitive behaviour has no real part of the complex power, as there is only the reactive contribution to the complex power, and Eq. (15) simplifies to

$$S(\omega) = jQ(\omega) = -\frac{j\Delta U_{rms}^2}{|Z''(\omega)|} = -j\omega C(\omega)\Delta U_{rms}^2. \tag{18}$$

System with the ideal $|Z''(\omega)|$ resistive behaviour has no imaginary part of the complex power as this component only dissipates energy and the complex power takes the well-known form

$$S(\omega) = \frac{\left|\Delta U_{\mathrm{rms}}\right|^2}{\left|Z'(\omega)\right|}. \tag{19}$$

It should be also noted that real EDLCs balances between the two states mentioned before: resistive at high frequencies ($f \to \infty$) and capacitive at low frequencies ($f \to 0$). Between these two states EDLC behaves like a resistive-capacitive (RC) transmission line equivalent circuit. The crossing of two plots appears when $|P| = |Q|$, i.e., when phase angle $\theta = -45°$, corresponding to the time constant τ_r ($\tau_r = 1/f_0$). This time constant has also been described as a dielectric relaxation time, which is a characteristic of the whole system. τ_r corresponds to the time required to release half of the energy stored in EDLC [23,25,26,34,54,57,59,61].

4.3.4. Maximum specific energy and power

The maximum specific energy, $E_{\max}$ (W h kg^{-1}), and power, $P_{\max}$ (kW kg^{-1}), for EDLCs can be calculated using Eqs. (20) and (21),

$$E_{\max} = \frac{C_s U^2}{2\, m_{tot}}, \tag{20}$$

$$P_{\max} = \frac{U^2}{4 R_s m_{tot}}, \tag{21}$$

where C_s is the series capacitance of the cell in F cm^{-2}, R_s is the equivalent series resistance in Ω cm^2 and m_{tot} is the mass of two electrodes in g. From Eqs. (20) and (21), it can be seen that the maximum voltage is an important parameter for determining both the specific energy and the power of EDLC [25,26,30,54–56].

5. EXPERIMENTAL

5.1. Electrospinning and separator materials characteristics

In present work, the electrospinning method has been used for preparation of the porous or fibrous polymer membranes. Electrospinning has been performed with different poly(vinylidene fluoride) (PVDF) polymer solutions at different electrospinning conditions to gain different polymer membranes. PVDF (with molecular weight 530 000 g mol^{-1}), N,N-dimethylformamide (DMF, 99.8%) and N,N-dimethylacetamide (DMA, 99.8%) were purchased from Fluka, and acetone from Sigma-Aldrich (puriss), all used without further purification. PVDF was selected as this polymer has a good processability, excellent mechanical properties and chemical stability. PVDF was dissolved in DMA or in DMF-acetone mixture (8:2,w:w) at room temperature in an ultrasonic bath to prepare the viscous polymer solution. The solution of PVDF was placed in a plastic syringe (5 ml) and fitted with a steel needle. Electrospinning was conducted at fixed electric field strength, which was generated with a high-voltage power supply system (ES40P-20W/DDPM, Gamma High Voltage Research Inc.). Syringe pump (ALADDIN-1000, World Precision Instruments) was used to feed the polymer solution into the tip of the needle. A grounded aluminium foil was located at a fixed distance from the needle tip to collect the formed fibers, which were randomly deposited onto the collector plate forming a fibrous thin membrane. Ten variable membranes, noted as TUX1–TUX3, TUX5, TUX7–TUX12, with different morphologies (porous or fibrious, Fig. 3) and thicknesses (from 10 to 38 μm) have been selected and studied more thoroughly. The detailed preparation conditions of self-made membranes are given in Table I.

To estimate the influence of the thickness of the separator materials on the electrochemical performance of EDLCs, the separators TUX1–TUX3 and TUX10–TUX12 have been cut out from the same porous or fibrous membranes, respectively, all having different thicknesses.

The surface structure of separators was examined using a FIB-SEM Helios™ Nanolab 600 or Microtrac Semtrac system. The electrospun nanofibers were sputter-coated with gold before the SEM observation. SEM micrographs of different separators are presented in Figures 3a–3h. Drastic morphological changes were found as a result of variation of the PVDF concentration in the solution, and electrospinning parameters (Figs. 3a–3f, Table I). In the case of TUX1–TUX3 and TUX5 separators (Figs. 3a and 3b) the mesomarcoporous melted structures were observed, mainly caused by the high PVDF concentration and fast polymer solution feed rate during the electrospinning process (Table I). In the SEM image for TUX7 (Fig. 3c) it can be seen that electrospun fibers started to merge together, caused by the high concentration of PVDF and low electric field strength applied. In the case of TUX8 and TUX9

separators (Figs. 3d and 3e) we prepared a compact structure of the beaded fibers and the fibers melted together, which is related to the instability of the jet of the polymer solution. From the SEM image for TUX10–TUX12 separators (Fig. 3f) we can see uniform electrospun fibers without any noticeable defects. Separator materials with different morphologies and porosities were selected to evaluate how these parameters influence the electrochemical performance of EDLCs [23–28].

Commercially available separator materials TF4425 (Nippon Kodoshi) and Celgard2400 (Celgard Co.) were also studied in order to estimate the suitability of the self-made membranes as separator materials for EDLC. TF4425 separator is prepared from cellulose and Celgard2400 from polypropylene, both having the thickness of nearly 25 μm. From the SEM images for the commercial TF4425 and Celgard2400 separators (Figs. 3g and 3h) it can be seen that the cellulose based separator has a fibrous and polypropylene separator has a complicated compact porous structure. These two commercial separators were selected as they are widely used in the energy storage systems and they have different chemical composition, i.e. different wettability. The cellulose based separator material is hydrophilic and insoluble in water as well as in most organic solvents. Although polypropylene based separator is very stable in different solvents, it has poor hygroscopicity and can have wetting problems.

Table I. Detailed preparation conditions of different PVDF separators [23–28].

Separator	Concentration of PVDF (%)	Solvent content	*dc* field strength (kV cm^{-1})	Polymer solution feed rate (ml h^{-1})	Distance between tip and collector (cm)
TUX1 TUX2 TUX3	20	DMA	0.70	15.0	25
TUX5	25	DMA	0.75	15.0	20
TUX7	25	DMF-acetone (8:2)	0.67	0.25	15
TUX8	20	DMF-acetone (8:2)	1.27	0.5	15
TUX9	20	DMF-acetone (8:2)	1.07	1.0	15
TUX10 TUX11 TUX12	22.5	DMF-acetone (8:2)	1.07	0.5	15

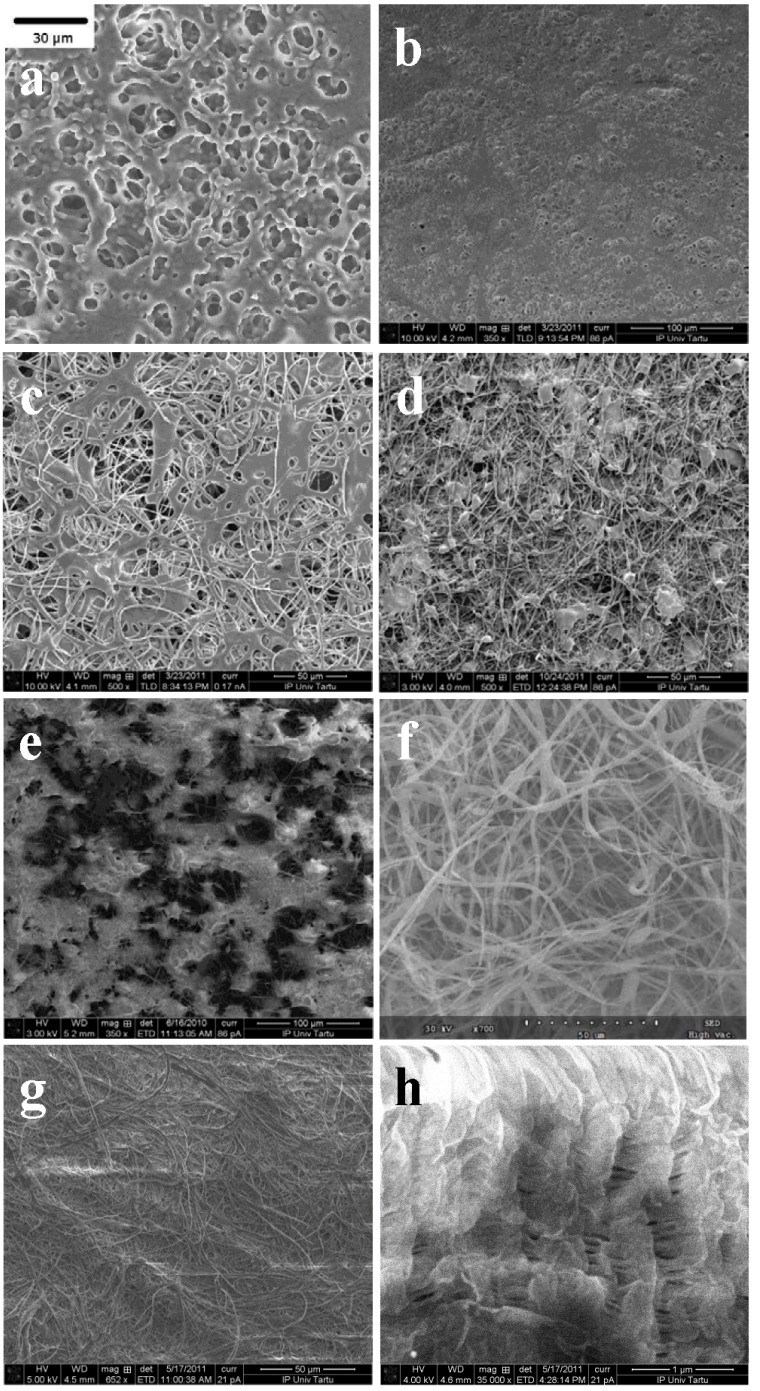

Figure 3. SEM images of a) TUX1–TUX3, b) TUX5, c) TUX7, d) TUX8, e) TUX9, f) TUX10–TUX12, g) TF4425 and h) Celgard2400 membranes.

Mercury intrusion porosimetry method was used to measure the pore size distribution, total surface area and total porosity of different separators. It was found that obtained pore size distribution, total surface area and total porosity of different separator materials depend noticeably on the separators preparation conditions (Figs. 4–7) as well as on the Hg pressure applied. The data for commercial separators, TF4425 and Celgard2400 have been added into Figures 4–7 for comparison. Data in Figure 4 inset, show that in the region of low Hg pressure ($p \leq 1000$ kPa), separators with more nanowire-nodal structure (TUX7, TUX8, TUX9, TUX10–TUX12 and TF4425) demonstrate higher surface area values than more compact TUX1–TUX3, TUX5, and Celgard2400 separators. However, at higher Hg pressures applied ($p > 3.5\times10^5$ kPa), the surface area values decrease in the different order: Celgard2400 > TUX10–TUX12 > TF4425 ≥ TUX5 > TUX7 ≥ TUX8 > TUX9 ≥ TUX1–TUX3. This information demonstrates that the nanowire-nodal point structural membranes are probably more compressible in real electrochemical exploitation conditions at pressure 981 kPa applied for completing the EDLC cell under current study. The values of specific surface area (S_{Hg}) and total porosity (P), given in Table II, have been calculated for the Hg pressure range from 1.37 to 4.1×10^5 kPa [25,28].

The total porosity of self-made separators decreases in the order: TUX1–TUX3 > TUX8 > TUX9 > TUX10–TUX12 > TUX7 > TUX5 (Table II). It can be seen, from the Figure 5a, that all separators with porous layered structure (TUX1–TUX3 and TUX5) have mainly pores with diameters from 10 to 1000 μm and there is only one main peak on the pore size distribution plot. Separators with more complicated nanowire-nodal point structure (TUX7, TUX8, TUX9 and TUX10–TUX12) have two main peaks on the pore size distribution plot (Fig. 5b): first main maximum within the range from 7 to 1000 μm and second main peak from 0.6 to 6 μm. Figures 5a and 5b show that for self-made separators there is a noticeable dependence of the pore size distribution on the solution composition (polymer concentration and solvent chemical composition) and electrospinning parameters (electric field strength) used. Commercially available separators have also two main peaks on the pore size distribution plot (Fig. 5a): for TF4425 first main maximum within the range from 9 to 1000 μm and second main peak from 0.4 to 2 μm, having more similar pore size distribution with self-made fibrous separators than Celgard2400, which has first main maximum within the range from 10 to 1000 μm and second main peak from 0.008 to 0.07 μm. The highest S_{Hg} for self-made separators has been obtained for TUX10–TUX12 separators (89.5 $m^2\ g^{-1}$) which, however, have medium porosity (24%) (Table II, Fig. 6) [25,28].

Table II. Mercury intrusion porosimetry measurement results [25,28].

Sample	S_{Hg} ($m^2\ g^{-1}$)	P (%)
TF4425	53.90	35
Celgard2400	120.50	4
TUX1–TUX3	21.15	42
TUX5	56.00	18
TUX7	37.84	23
TUX8	32.25	30
TUX9	26.50	26
TUX10–TUX12	89.50	24

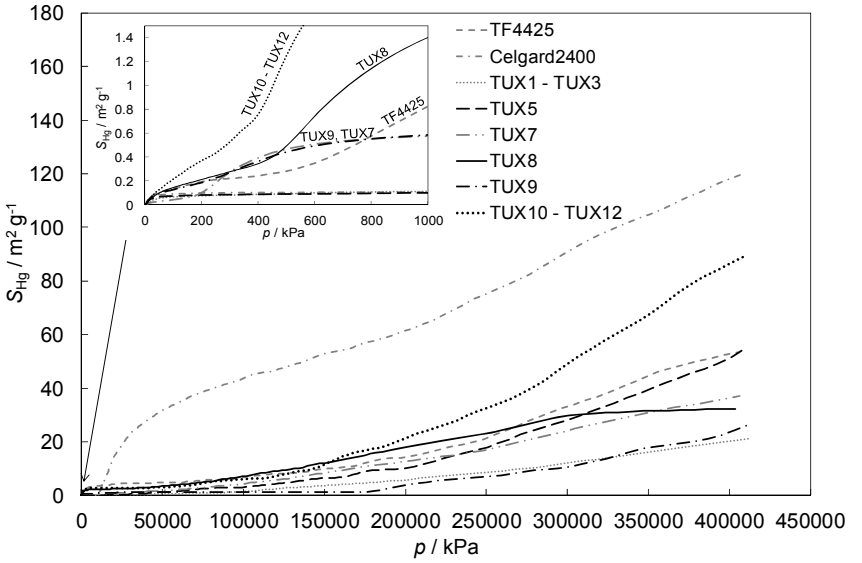

Figure 4. Surface area vs. pressure dependencies for different separator materials (noted in figure).

Data in Figure 6 demonstrate that the total porosity of a material depends on the separator material structure and for self-made separators with more nanowire structure (TUX7, TUX8, TUX9 and TUX10–TUX12) two plateaus can be seen on porosity vs. pore diameter plots: first plateau in the wider pore diameter region and second in the smaller pore diameter region. Figure 7 demonstrates that in the region of low Hg pressure ($p \leq 300$ kPa), there is a very well expressed influence of the physical properties of the separator material on the obtained porosity. However, at higher Hg pressures at $p > 1200$ kPa, porosity is practically independent of p applied [25,28].

Differential scanning calorimetry measurements were performed in order to determine the thermal stability of PVDF membranes and it was found that all self-made separators meet the requirements of separator thermal stability ($T_{melt} \geq 140$ °C).

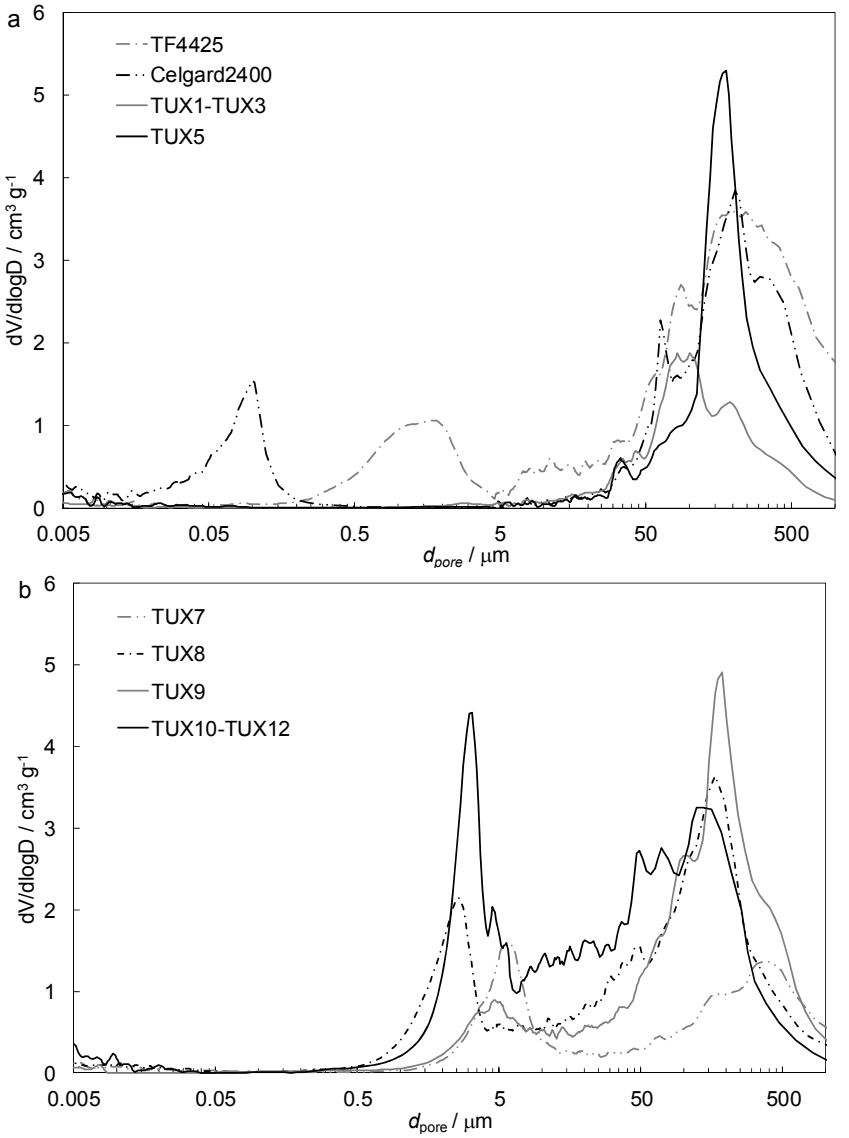

Figure 5. Differential pore size distribution dV/dlog$D$ vs. pore diameter dependencies for different separator materials (noted in figures).

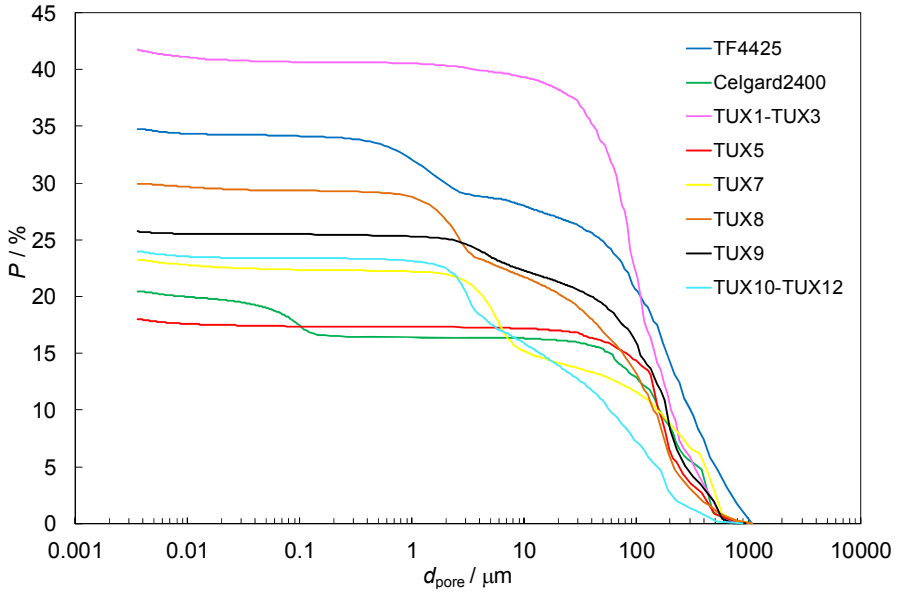

Figure 6. Porosity vs. pore diameter dependencies for different separator materials (noted in figure).

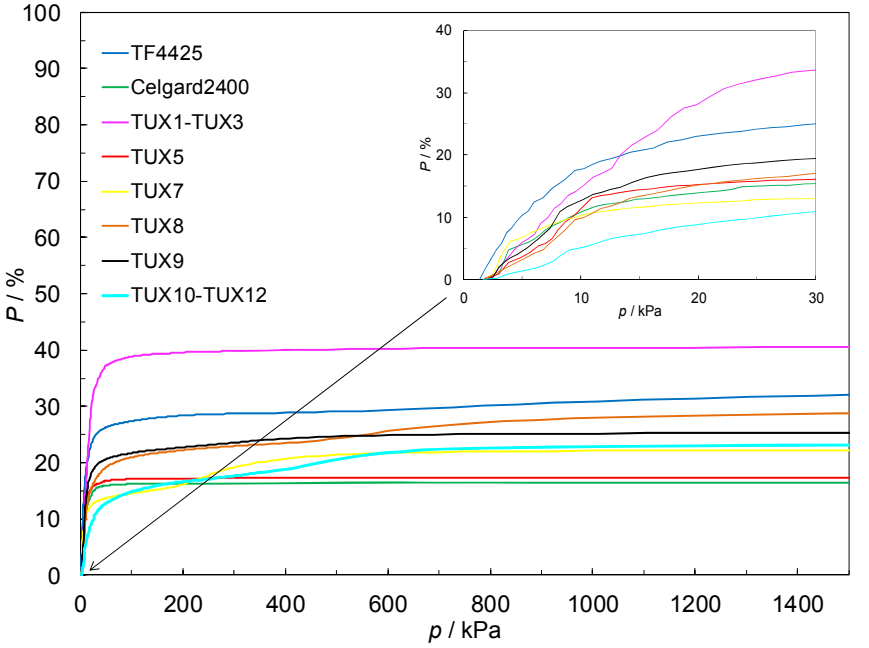

Figure 7. Porosity vs. pressure dependencies for different separator materials (noted in figure).

5.2. Electrode materials and preparation of electrodes

In present work two different electrode materials with different thicknesses were used for completing the EDLC cells, both prepared from TiC derived carbon (TiC-CDC), synthesized at 950 °C according to the preparation scheme discussed in References [49,54]. For some EDLC cells, the 120 ± 5 μm thick (i) [23,25,27] electrode material consisting of TiC (Alfa Aesar, USA), noted as TiC-CDC-1 and for others EDLC cells the 105 ± 5 μm thick (ii) [24,26,28] electrode material consisting of TiC (Aldrich ~325 mesh, Germany), noted as TiC-CDC-2, were used. The active layer of the electrode consists mainly of the micromesoporous carbon particles and of the binder (polytetrafluoroethylene, 60% dispersion in H_2O, Sigma-Aldrich), pressed together to form a flexible layer of the active electrode material. The electrode material was covered by pure Al layer (3 μm) from one side by the plasma activated physical vapour deposition method.

For surface area and porosity analysis of the electrode materials, the N_2 adsorption was measured at 77 K using the ASAP 2020 (Micromeritics, USA) gas adsorption measurement system. The parameters have been calculated from N_2 adsorption isotherms according to Brunauer-Emmett-Teller (BET), *t*-plot method and non-local density functional theory [23–27]. The data measured demonstrate that both synthesised TiC-CDC materials have high surface area and are mainly microporous materials (Table III) [23–26,28,49].

Table III. Results of sorption measurements of Ti-CDC.

Microporous carbon	S_{BET} ($m^2\ g^{-1}$)	S_{micro} ($m^2\ g^{-1}$)	V_{micro} ($cm^3\ g^{-1}$)	V_{tot} ($cm^3\ g^{-1}$)
TiC-CDC-1	1863	1685	0.76	1.01
TiC-CDC-2	1525	1455	0.63	0.79

S_{BET} – specific surface area calculated by Brunauer-Emmett-Teller theory (p/p_0 = 0.05…0.2); S_{micro} – micropore specific surface area calculated by *t*-plot method; V_{micro} – micropore volume calculated by *t*-plot method; V_{tot} – total pore volume at p/p_0 = 0.999.

5.3. Electrolytes

For comprehensive analysis of the influence of the separator properties on EDLC parameters, three different non-aqueous electrolytes were used: 1 M triethylmethylammonium tetrafluoroborate ($TEMABF_4$) in acetonitrile (AN), 1 M $TEMABF_4$ in dimethyl carbonate, ethylene carbonate and propylene carbonate (DMF+EC+PC) mixture with 1:1:1 volume ratio, and room temperature ionic liquid (RTIL) 1-ethyl-3-methylimidazolium tetrafluoroborate ($EMImBF_4$). AN has been selected for experiments because this solvent has very high molar conductivity, high relative macroscopic dielectrical permittivity

and dipole moment (vertical component) value and AN is stable within the very wide region of cell voltage applied. DMF+EC+PC mixture was selected because the EDLCs based on this solvent mixture are able to work even at very low temperatures (–30 °C). Room temperature ionic liquid was used because it has a wide region of electrical stability, good conductivity but higher viscosity than previously mentioned electrolytes.

5.4. Wetting properties of the separator materials in different electrolytes

The wetting angle of different separators with different electrolytes was investigated to determine the chemical compatibility between the separator material and the electrolyte. It was found that in 1 M $TEMABF_4$ + AN solution all separators, except Celgard2400, were nicely wetted (Figs. 8a and 8b). Also in the case of 1 M $TEMABF_4$ in DMF+EC+PC mixture, we notice some wetting problems only with Celgard2400 separator (Figs. 9a–9d). The biggest wetting problem was observed in the case of $EMImBF_4$, as this is the most viscous electrolyte under study. It was found that Celgard2400 separator did not wet at all in RTIL and some wetting problems occurred with TF4425 as well as with self-made very compact only slightly porous TUX5 separator (Figs. 10a–10d).

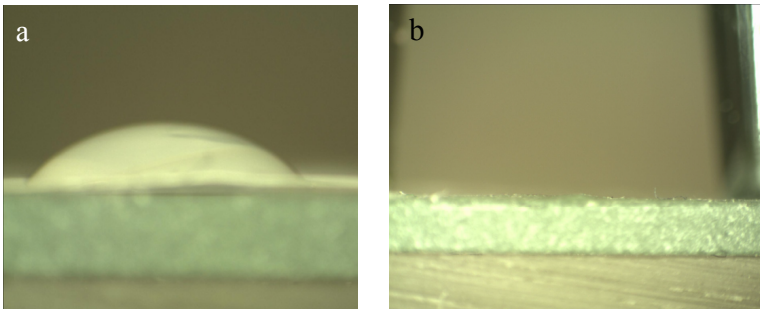

Figure 8. Microscopic images of the wetting angle for a) Celgard2400 and b) TUX5 separators with 1 M $TEMABF_4$ + AN electrolyte.

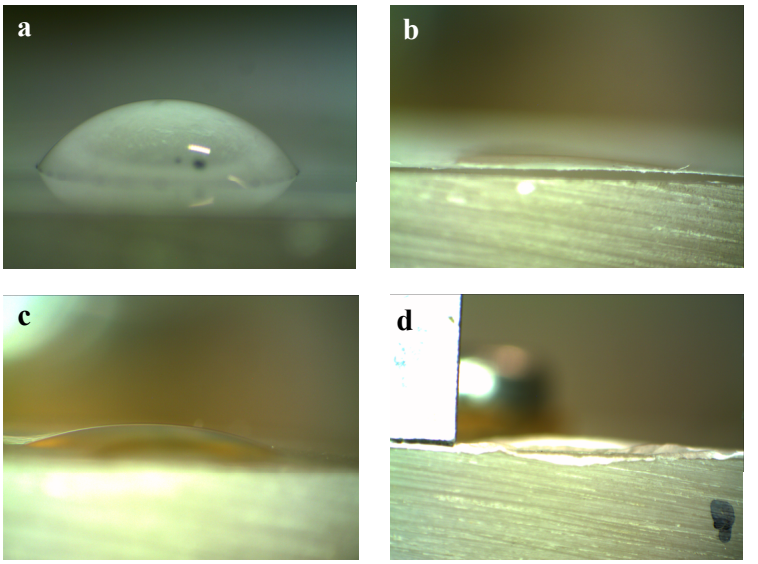

Figure 9. Microscopic images for the wetting angle of a) Celgard2400, b) TF4425, c) TUX5 and d) TUX10 separators with 1 M $TEMABF_4$ in DMF+EC+PC electrolyte.

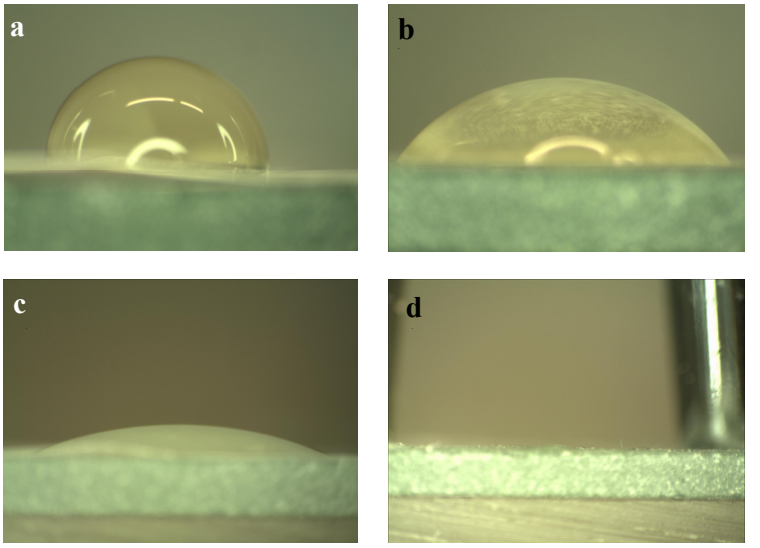

Figure 10. Microscopic images for the wetting angle of a) Celgard2400, b) TUX5, c) TF4425 and d) TUX10 separators with $EMImBF_4$.

5.5. Assembling EDLC test cells and electrochemical measurements

The cell components (separator sheet between two identical electrodes with geometric surface area of one electrode $S_{electrode}$ = 2 cm^2) and electrolyte solution were set into a hermetic aluminium test cell (HS Test Cell, Hohsen Corporation Japan) inside the glove box (Labmaster sp, MBraun, Germany; O_2 and H_2O concentrations lower than 0.1 ppm) under constant contact spring pressure of 20 kg to ensure the good electrical contact.

Different separators with different thicknesses were used to complete the EDLC cells with different electrolytes (Table IV). Commercially available separator materials TF4425 and Celgard2400 were also investigated at the same conditions as the self-made separators to estimate suitability of the self-made membranes as a separator material for EDLC.

Table IV. Thicknesses of the separator materials [23–27].

Separator / Electrolyte	1M $TEMABF_4$ + AN	1M $TEMABF_4$ + (DMF+EC+PC)	$EMImBF_4$
TF4425	25 μm	25 μm	25 μm
Celgard2400	25 μm	25 μm	–
TUX1	15 μm	–	–
TUX2	22 μm	–	–
TUX3	33 μm	–	–
TUX5	10 μm	10 μm	14 μm
TUX7	26 μm	–	17 μm
TUX8	38 μm	–	25 μm
TUX9	31 μm	–	24 μm
TUX10	–	20 μm	14 μm
TUX11	–	–	18 μm
TUX12	–	–	26 μm

The electrochemical behavior of EDLCs was tested with cyclic voltammetry and electrochemical impedance spectroscopy methods using a Solartron 1287 potentiostat with a 1252A frequency response analyser. Impedance spectra were recorded over an *ac* frequency (f) range from 3×10^5 to 1×10^{-3} Hz using 5 mV *ac* modulation. Constant power discharge tests were performed with a BT2000 testing system (Arbin Instruments, USA). Electrochemical measurements were carried out at temperature T = 23 ± 0.5 °C, if not pointed otherwise.

6. RESULTS AND DISCUSSION

6.1. Influence of the separator materials properties on the electrochemical behaviour of EDLCs [I–VI]

In order to study the influence of separator material properties (chemical composition, wettability, porosity, thickness) on the performance of EDLCs, 7 different separators were selected (TF4425, Celgard2400, TUX5, TUX7–TUX10), having different chemical compositions, morphologies, porosities, and thicknesses. Electrochemical measurements with different separators were carried out at room temperature in three different electrolytes, to study also the influence of chemical compatibility and wetting of separators with different electrolytes applied.

6.1.1. Cyclic voltammetry data

The CV method has been employed to estimate the ideal polarizability region of different EDLC cells. The cyclic voltammograms were measured applying the voltage scan rate varied from 1 to 100 mV s^{-1} to EDLC cells completed with different separators and electrolytes. The cyclic voltammograms presented in Figures 11a–11c show that for all EDLCs the so-called ideal capacitive behaviour has been established at voltage scan rate 1 mV s^{-1} and at cell voltage $U \leq 3.2$ V. However, from the Figures 12a–12c, it can be observed that at higher voltage scan rates the so-called distortion effects can be seen in the region of voltage switchover for all systems studied. The influence of separator materials properties on the shape of cyclic voltammograms is clearly demonstrated in the case of RTIL based EDLC cells (Fig. 12c), where the nearly ideal capacitive behavior has been established at scan rate $v \leq 10$ mV s^{-1} only for systems completed with TUX7, TUX9 and TUX10 separators, which are less compact than TUX5 and TF4425 separators.

It is very surprising that there is only a very weak dependence of current (j) on the separator material used, if slow voltage scan rates ($v \leq 5$ mV s^{-1}) are used. However, at $v \geq 10$ mV s^{-1}, there is a dependence of j on the thickness, porosity, and chemical composition of separator material studied and this effect is more noticeable for EDLCs containing RTIL (more viscous electrolyte).

Analysis of the experimental data (Figs. 13a–13c) demonstrates that the values of specific capacitance C_m, calculated from cyclic voltammograms according to Equations (2) and (3), are practically independent of separator material, if the slow voltage scan rates are applied ($v \leq 5$ mV s^{-1}) and are mainly determined by the electrode material properties. At higher scan rates $v \geq 10$ mV s^{-1}, there is a dependence of C_m on the thickness, porosity, and chemical composition of separator material studied, especially for EDLCs, which are completed using a more viscous electrolyte.

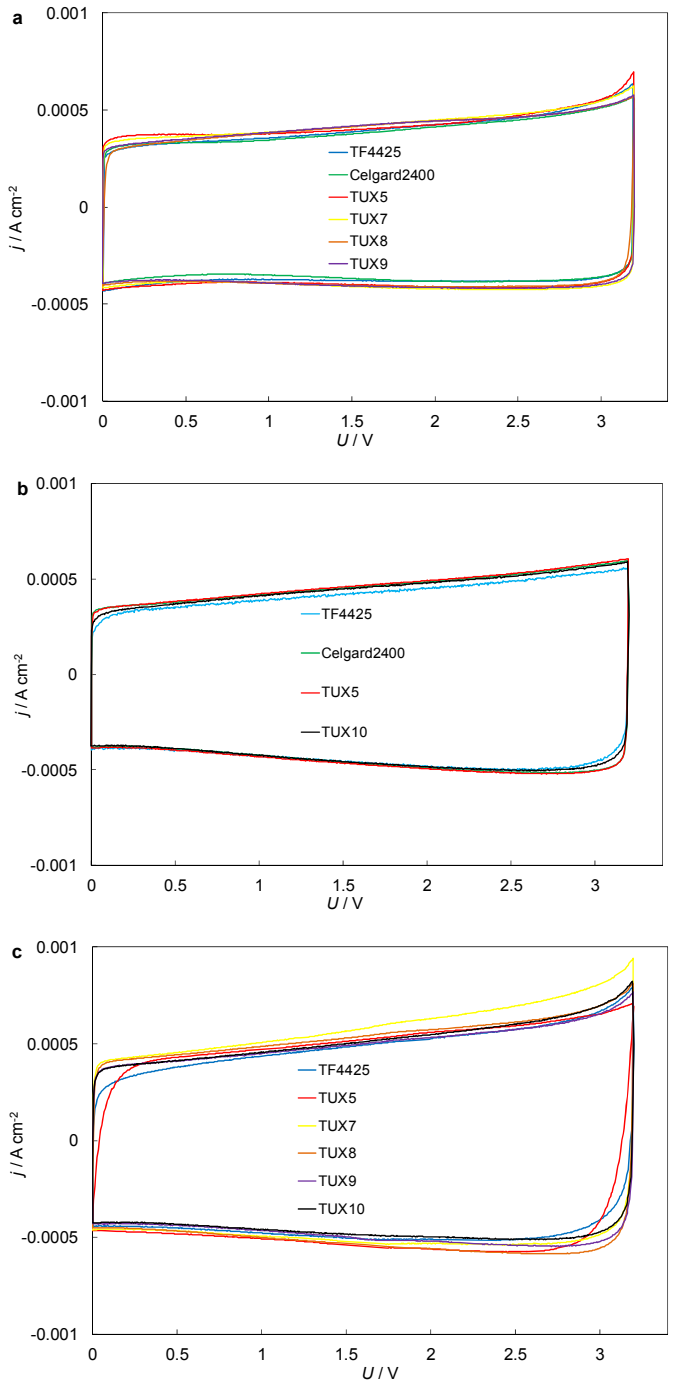

Figure 11. Cyclic voltammograms for EDLCs based on different separators (noted in figures) measured with voltage scan rate 1 mV s^{-1} up to 3.2 V in different electrolytes: a) 1 M $TEMABF_4$ + AN, b) 1 M $TEMABF_4$ + (DMF+EC+PC) and c) $EMImBF_4$.

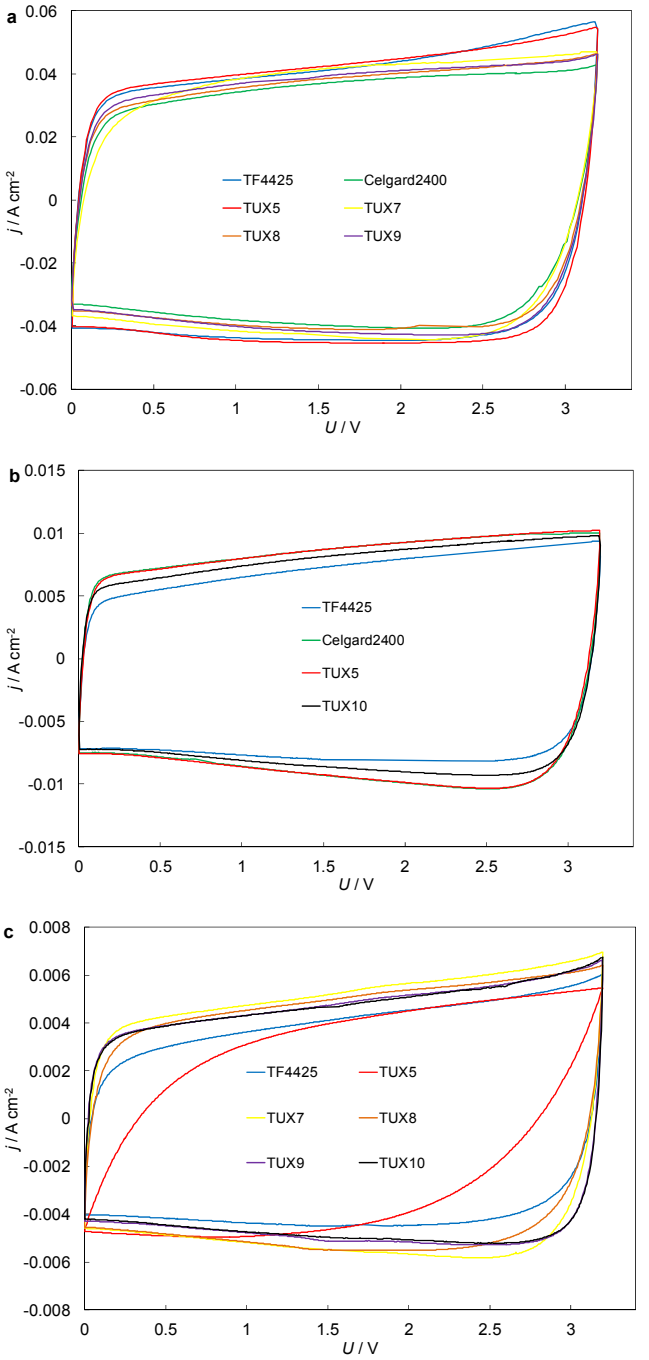

Figure 12. Cyclic voltammograms for EDLCs based on different separators (noted in figures) in different electrolytes and measured with different voltage scan rates: a) in 1 M TEMABF$_4$ + AN, v = 100 mV s^{-1}, b) in 1 M TEMABF$_4$ + (DMF+EC+PC), v = 20 mV s^{-1} and c) in EMImBF$_4$, v = 10 mV s^{-1}.

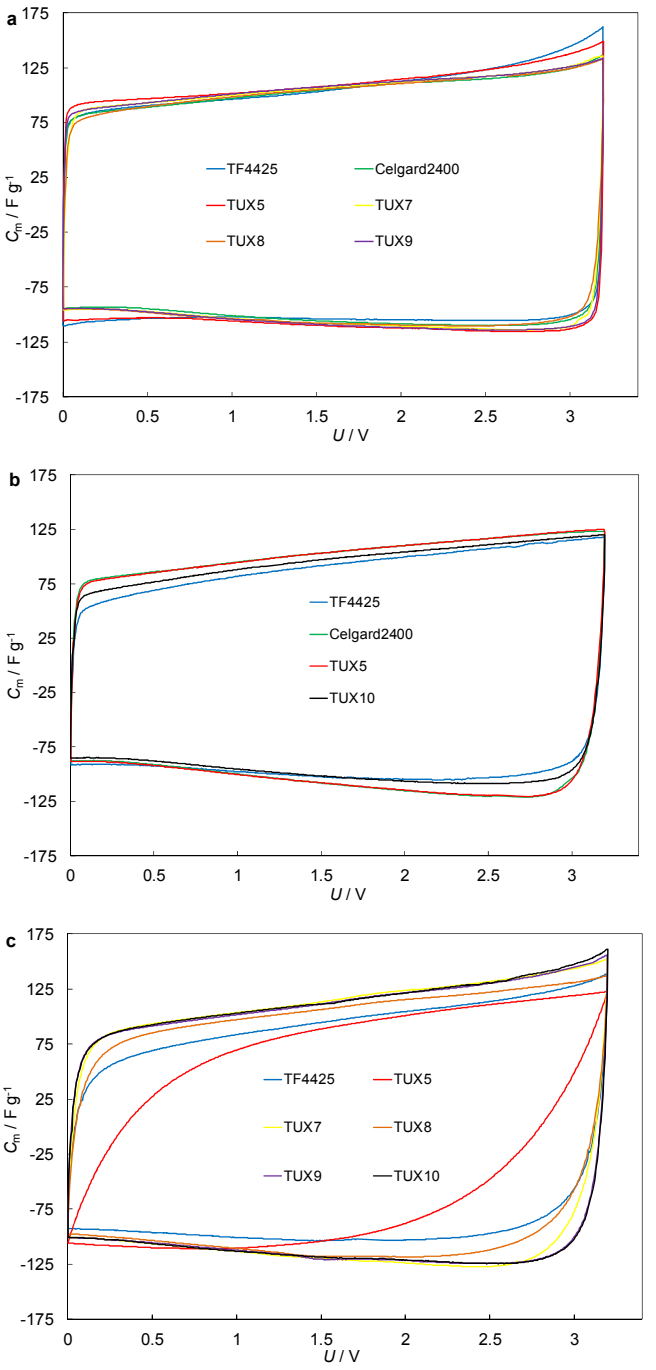

Figure 13. Specific capacitance vs. cell voltage for EDLCs, based on different separators (noted in figures) measured with voltage scan rate 10 mV s^{-1} and in different electrolytes: a) 1 M $TEMABF_4$ + AN, b) 1 M $TEMABF_4$ + (DMF+EC+PC) and c) $EMImBF_4$.

6.1.2. Electrochemical impedance spectroscopy data

The impedance complex plane (Z'' vs. Z'), i.e. Nyquist plots, for EDLC cells with different separators and electrolytes are given in Figures 14a–14c. Extrapolation of the high frequency part of the Z'' vs. Z' dependence to the condition $Z''(\omega) = 0$ gives the so-called equivalent series resistance of the cell $Z'(\omega\rightarrow\infty)=R_s(\omega\rightarrow\infty)$, being the sum of contact resistance at carbon|Al current collector interface, series resistance between carbon particles inside the carbon electrode, electrolyte series resistance inside the porous electrode matrix and separator, etc. As the electrode composition, current collectors and electrolyte concentration were fixed, therefore, the variation in very high frequency series resistance values can be explained mainly by the different separator material parameters. According to the data in Figures 14a–14c, $R_s(\omega\rightarrow\infty)$ depends noticeably on the used separator material, thus, mainly on the conductivity of an electrolyte inside the porous separator matrix, characterised by different chemical composition, total porosity, specific surface area and pore size distribution (Figs. 4–7 and Table II), discussed above. Unfortunately, there is not yet an easy explanation how the total porosity, specific surface area and pore size distribution influence the $R_s(\omega\rightarrow\infty)$ value. $R_s(\omega\rightarrow\infty)$ is a very complex parameter depending strongly on the separator material and electrolyte chemical compatibility and, therefore, is mainly influenced by the microwetting process of a membrane. It should be noted that in the case of Celgard2400 separator in acetonitrile and carbonate mixture based systems, the strongly depressed very small semicircle can be seen in the region of high and medium *ac* frequenies ($300 < f < 300\,000$ Hz) (Figs. 13a and 13b), dependent mainly on the electrolyte resistance inside the separator material matrix. This can be explained by the fact that polypropylene has very poor wettability and the separator microwetting problems are prevailing over other $R_s(\omega\rightarrow\infty)$ components. The strongly depressed semicircle can also be seen in the case of EDLC completed with TUX5 separator in carbonates mixture and RTIL based systems (Figs. 14b and 14c), which is caused mainly by poor wettability of TUX5 separator with the more viscous electrolytes.

It was found that there is a strong dependence of phase angle (θ) on the separator material characteristics in the region of *ac* frequency from 0.02 to 10 Hz (Fig. 15), which is caused by the differences in ionic conductivity of the electrolyte ions inside the porous separator material, obtaining the differences in characteristic time constants of the cells under study. At $f \approx 0.01$ Hz, all the investigated systems have nearly ideal capacitive behaviour ($\theta \leq -87$) (Fig. 15).

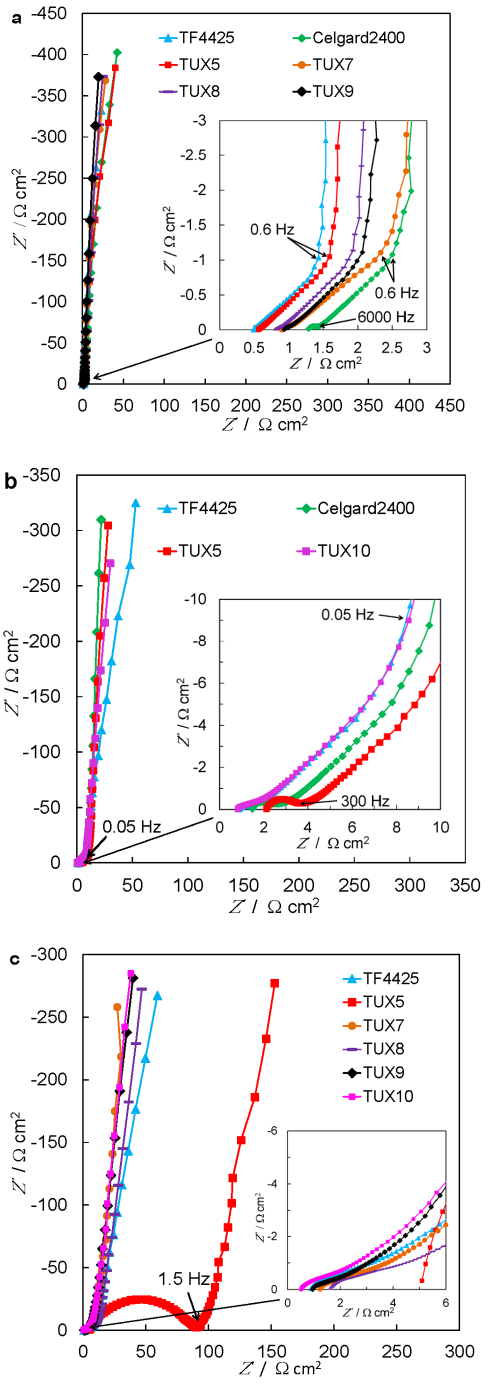

Figure 14. Complex impedance plane plots for the EDLC cells, completed with different separator materials (noted in figures) in: a) 1 M $TEMABF_4$ + AN solution at 3.0 V, b) 1 M $TEMABF_4$ + (DMF+EC+PC) at 3.0 V and c) $EMImBF_4$ at 3.2 V.

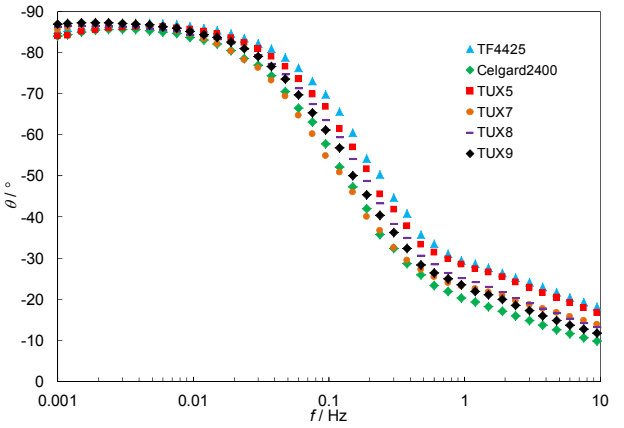

Figure 15. Phase angle vs. *ac* frequency plots for the EDLC cells completed using different separators (noted in fiqure) in 1 M $TEMABF_4$ + AN solution at cell potetntial 3.0 V.

The dependencies of the C_p/C_s ratio on frequency are shown in Figures 16a and 16b. For an ideally polarizable system, the ratio $C_p/C_s = 1$, which can be seen for all EDLCs under study, except for EDLC completed with TUX5 separator in RTIL. In the case of EDLC completed with TUX5 separator in RTIL, the C_p/C_s ratio plateau is not achieved even at very low ac frequency $f = 0.001$ Hz, caused mainly by the very slow mass transfer rate of the ions inside the very compact separator material matrix, which may have some microwetting problems. For the systems completed with TUX8 and TF4425 separators in RTIL, the C_p/C_s ratio starts to decrease slightly (Fig. 16b), indicating the slow mass transfer rate of the ions inside the separator matrix, which is caused by the higher viscosity of the electrolyte used. The noticeable dependence of C_p/C_s ratio on *ac* frequency at $f > 2\times10^{-2}$ Hz for EDLCs completed using different separators can be explained by the influence of the separator material porosity and structure on the values of series C_s and R_s for a two electrode EDLC cell under study. It was demonstrated that the EDLCs containing less viscous electrolyte (1 M $TEMABF_4$ + AN solution, Fig. 16a) achieve the maximum C_p/C_s ratio much faster than the EDLC based on viscous $EMImBF_4$ electrolyte.

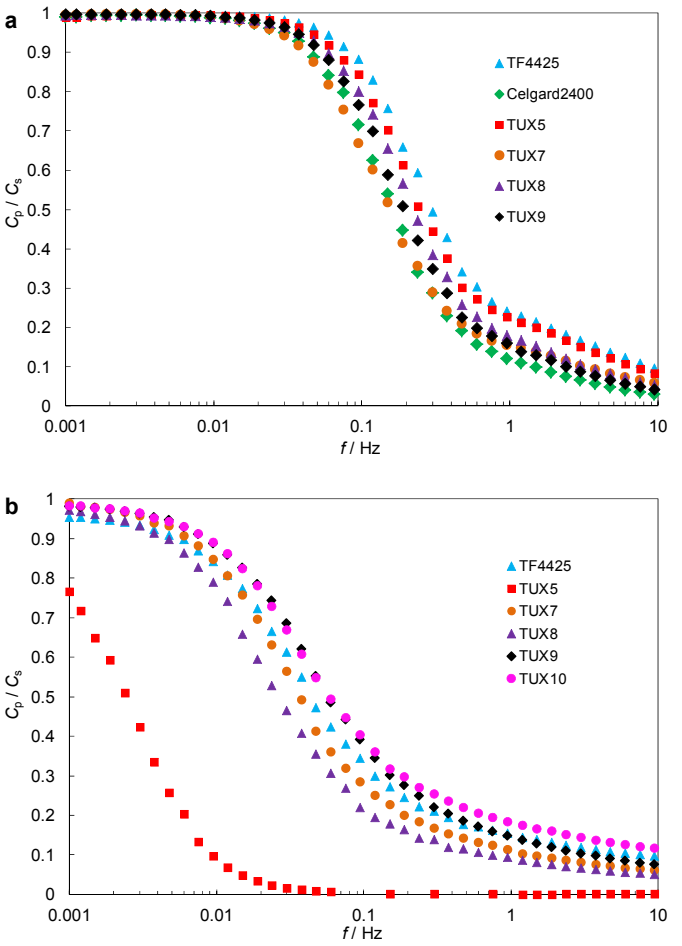

Figure 16. C_p/C_s ratio vs. *ac* frequency dependencies for the EDLCs completed using different separator materials (noted in figure) in: a) 1 M $TEMABF_4$ + AN solution at 3.0 V and b) $EMImBF_4$ at 3.2 V.

The dependencies of the normalised real part ($|P|/|S|$) and imaginary part ($|Q|/|S|$) of the complex power on *ac* frequency for different EDLCs can be seen on the Figures 17–17c. Comparison of the data for the cells completed using different separators and electrolytes indicates the noticeable influence of the separator properties on the characteristic time constant τ_R values. Thus, the chemical composition, wetting ability, porosity, specific surface area and thickness of the separator, i.e. in reality the series resistance of the electrolyte in the porous separator, has a noticeable influence on the characteristic time constant, obtained at the condition $|Q|/|S| = |P|/|S|$.

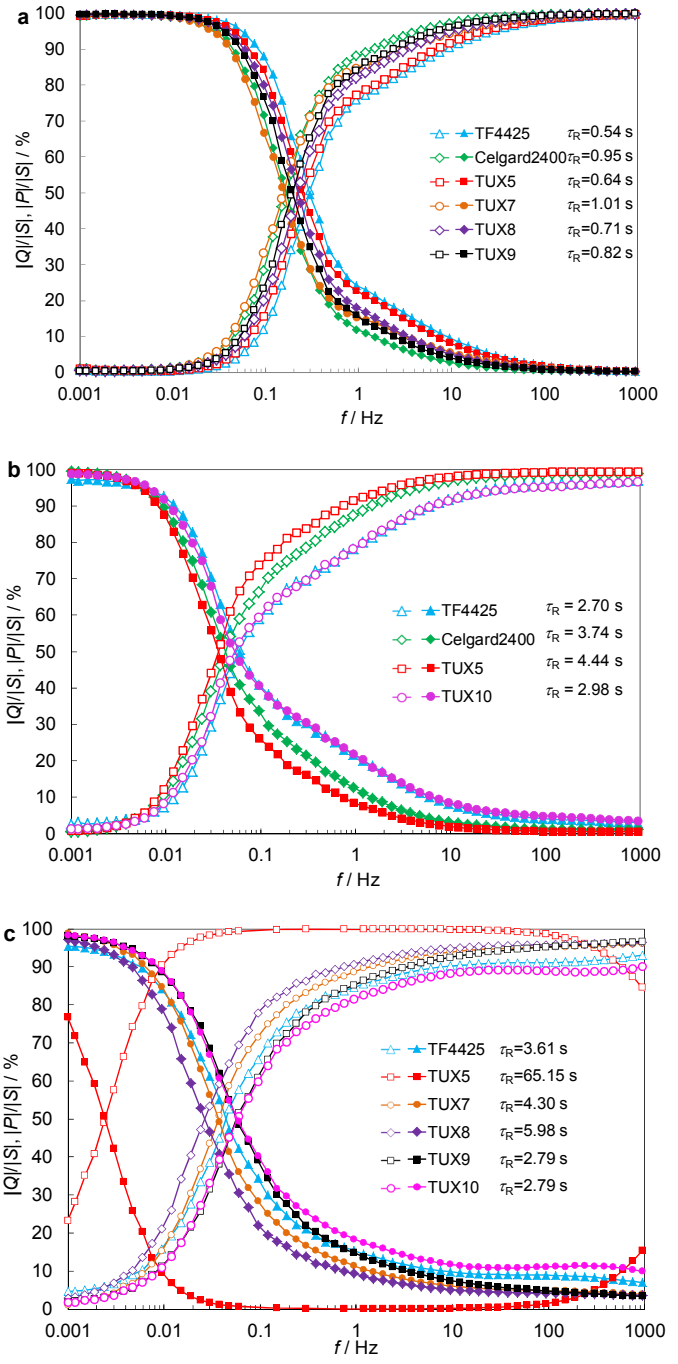

Figure 17. Normalized reactive power $|Q|/|S|$ (filled marks), and active power $|P|/|S|$ (open marks) vs. *ac* frequency plots for EDLCs completed using different separator materials (noted in figures) in: a) 1 M $TEMABF_4$ + AN at 3.0 V, b) 1 M $TEMABF_4$ + (DMF+EC+PC) at 3.0 V, and c) $EMImBF_4$ at 3.2 V.

6.1.3. Maximum specific energy and power plots

The maximum specific energy (E_{max}) and power (P_{max}) values have been calculated according to the Equations 20 and 21 and are represented in Table V and VI, respectively. It was found that E_{max} weakly depends on the separator material chemical composition and its ability to be wetted by the electrolyte. Thus, the E_{max} for fully charged/discharged system is determined mainly by the microporous TiC-CDC electrode material properties. However, P_{max} depends noticeably on the separator material parameters (chemical composition, wettability by the electrolyte, porosity, specific surface area, pore size distribution), thus, on the conductivity of the electrolyte in the separator matrix. By varying separator materials inside EDLC system, it is possible to increase the specific power values without sacrificing noticeably in the specific energy values.

Table V. The maximum specific energy (E_{max}) for different EDLCs at 3.0 V, calculated from impedance data.

Electrolyte / Separator	1 M $TEMABF_4$ + AN	1 M $TEMABF_4$ + DMC+EC+PC	$EMImBF_4$
TF4425	33.2 Wh kg^{-1}	41.7 Wh kg^{-1}	33.9 Wh kg^{-1}
Celgard2400	29.9 Wh kg^{-1}	42.6 Wh kg^{-1}	–
TUX5	34.0 Wh kg^{-1}	43.2 Wh kg^{-1}	39.0 Wh kg^{-1}
TUX7	33.1 Wh kg^{-1}	–	38.8 Wh kg^{-1}
TUX8	31.7 Wh kg^{-1}	–	38.6 Wh kg^{-1}
TUX9	33.4 Wh kg^{-1}	–	39.1 Wh kg^{-1}
TUX10	–	40.7 Wh kg^{-1}	40.5 Wh kg^{-1}

Table VI. The maximum specific power (P_{max}) for different EDLCs at 3.0 V, calculated from impedance data.

Electrolyte / Separator	1 M $TEMABF_4$ + AN	1 M $TEMABF_4$ + DMC+EC+PC	$EMImBF_4$
TF4425	305 kW kg^{-1}	173 kW kg^{-1}	153 kW kg^{-1}
Celgard2400	106 kW kg^{-1}	102 kW kg^{-1}	–
TUX5	264 kW kg^{-1}	71 kW kg^{-1}	25 kW kg^{-1}
TUX7	159 kW kg^{-1}	–	104 kW kg^{-1}
TUX8	180 kW kg^{-1}	–	75 kW kg^{-1}
TUX9	160 kW kg^{-1}	–	143 kW kg^{-1}
TUX10	–	181 kW kg^{-1}	258 kW kg^{-1}

6.1.4. Constant power discharge test results

The experimental specific energy and power relationship has been obtained from constant power discharge tests within the cell voltage range from 3.0 V to 1.5 V (Figs. 18a and 18b). The Ragone plots for different EDLCs at moderate power densities noticeably depend on the separator properties used. Thus, the attainable specific power of EDLCs depends noticeably on the separator parameters used, i.e. being higher for EDLCs based separators, which are wetted more easily by the electrolyte. By varying and optimizing the separator material parameters (chemical composition, wettability, porosity, thickness), it is possible to increase remarkably the specific power value for an EDLC system.

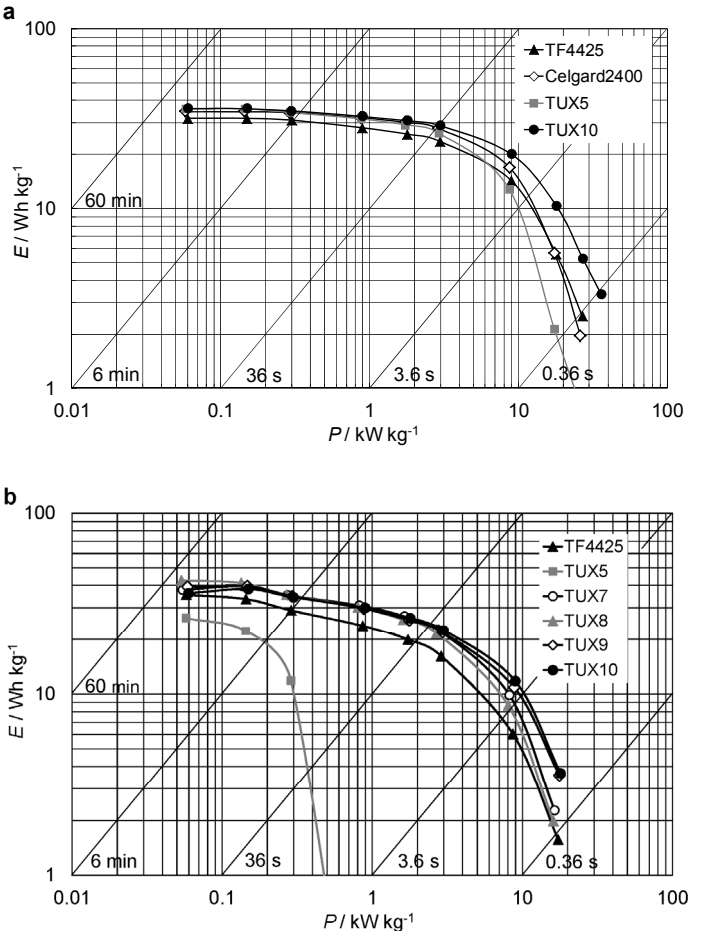

Figure 18. Ragone plots for EDLCs completed using different separators (noted in figures) in: a) 1 M $TEMABF_4$ + (DMC+EC+PC) and b) $EMImBF_4$.

6.2. Influence of the separator thickness on the electrochemical behaviour of EDLCs [I,II]

Two different separator materials (porous and fibrous) with 3 different thicknesses were selected to study the influence of separator material thickness on the performance of EDLCs [23,24]. EDLCs completed with porous separators TUX1 (15 μm), TUX2 (22 μm) and TUX3 (33 μm) (Fig. 3a) and 1 M $TEMABF_4$ + AN solution, and systems completed with fibrous separators TUX10 (14 μm), TUX11 (18 μm) and TUX12 (26 μm) (Fig. 3f) and $EMImBF_4$ were measured at room temperature.

6.2.1. Cyclic voltammetry data

The cyclic voltammograms were measured applying the voltage scan rate, varied from 1 to 100 mV s^{-1}, to EDLC cells completed with separators of different thicknesses. The cyclic voltammograms presented in Figures 19a and 19b show that the so-called ideal capacitive behaviour has been established for all EDLCs at voltage scan rate 1 mV s^{-1}.

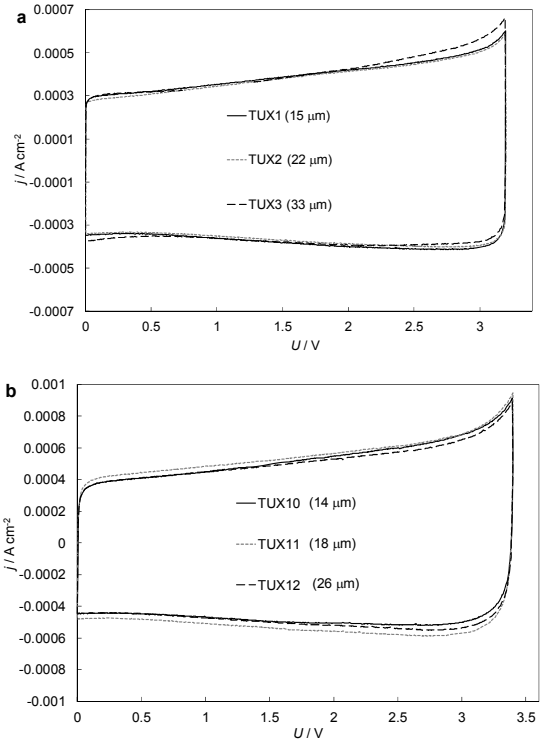

Figure 19. Cyclic voltammograms for EDLCs based on different separators (noted in figures) measured at voltage scan rate 1 mV s^{-1} in different electrolytes: a) 1 M $TEMABF_4$ + AN up to 3.2 V and b) $EMImBF_4$ up to 3.4 V.

It has been observed that the separator thickness has a little influence on the shape of the cyclic voltammograms, even when higher voltage scan rates have been used (Figs. 20a–20b). Thus, separator materials thickness has a little influence on the specific capacitance values, if a good chemical compatibility (wettability) has been achieved between the separator material and the electrolyte.

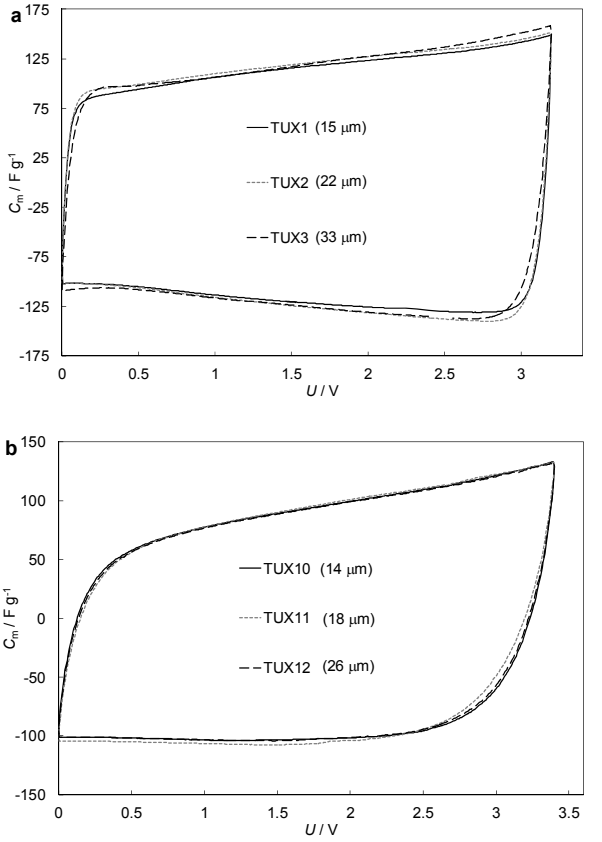

Figure 20. Specific capacitance for EDLCs based on separators with different thicknesses (noted in figures) measured with scan rate 50 mV s^{-1} in different electrolytes: a) 1 M $TEMABF_4$ + AN up to 3.2 V and b) $EMImBF_4$ up to 3.4 V.

6.2.2. Electrochemical impedance spectroscopy data

The impedance complex plane plots for EDLC cells, completed with separators of different thicknesses, are given in Figures 21a and 21b. It can be seen that the equivalent series resistance of the cell increases with the increase of the thickness of the separators used (Figs. 21a–21b). In the case of EDLCs completed with compact porous separators (TUX1–TUX3) in 1 M $TEMABF_4$ + AN solution

the strongly depressed very small semicircles can be seen in the region of high and medium *ac* frequencies ($1500 < f < 300\,000$ Hz). It is important to notice that the size of the strongly depressed semicircles increase with increasing the thickness of the separator material (Fig. 21a), demonstrating briefly that the wideness of the semicircle depends on the mass transfer process resistance at/inside of the porous separator.

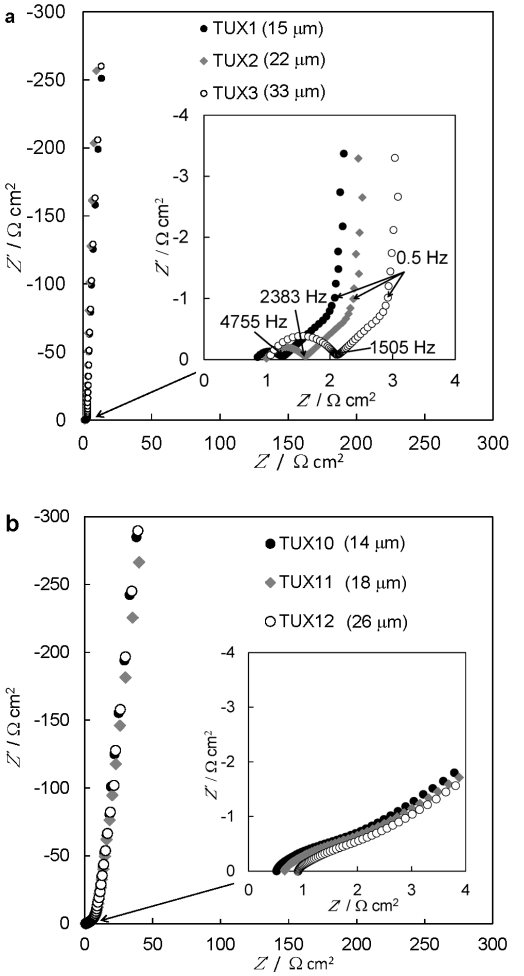

Figure 21. Complex impedance plane plots for the EDLC cells, completed with separators of different thicknesses (noted in figures) in: a) 1 M $TEMABF_4$ + AN solution at 3.0 V and b) $EMImBF_4$ at 3.2 V.

It was found that the separator material thickness has little influence on the phase angle value in the region of low *ac* frequency $f \leq 0.02$ Hz. However, there is a strong dependence of the phase angle on the thickness of separator material

within the region of *ac* frequency from 0.02 to 10 Hz (Fig. 22), which is caused by the differences in ionic conductivity of the electrolyte ions inside the porous separator material, determing the differences in characteristic time constants of the cells under study.

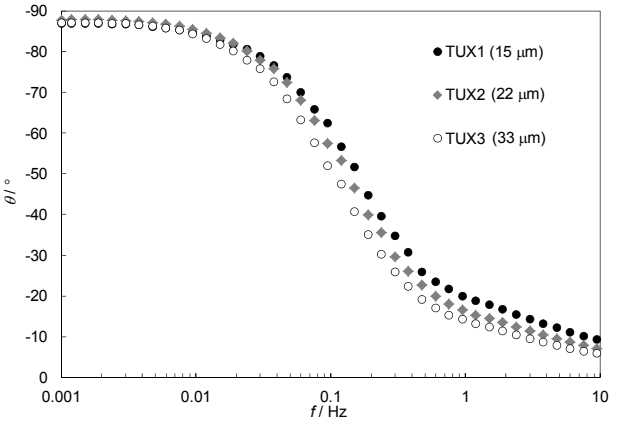

Figure 22. Phase angle vs. *ac* frequency plots for the EDLC cells completed with separators of different thicknesses (noted in figure) in 1 M $TEMABF_4$ + AN solution at cell potential 3.0 V.

The dependencies of the C_p/C_s ratio on *ac* frequency is shown in Figure 23, and at $f > 5\times10^{-2}$ Hz, the very noticeable dependence of C_p/C_s on f can be explained by the influence of separator material thickness on the series C_s and R_s values. Thus, EDLCs with thinner separator material show shorter characteristic charging/discharging times than EDLCs completed with thicker separators, having higher R_s values.

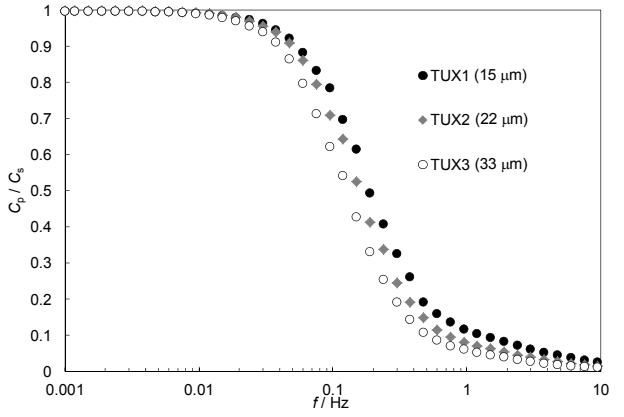

Figure 23. C_p/C_s ratio vs. *ac* frequency dependencies for the EDLCs completed using separators of different thicknesses (noted in figure) in 1 M $TEMABF_4$ + AN solution at 3.0 V.

The dependencies of the normalised real part ($|P|/|S|$) and imaginary part ($|Q|/|S|$) of the complex power on *ac* frequency plots are presented in Figures 24a and 24b. Comparison of the data indicates the noticeable influence of the separator thickness on the characteristic time constant values obtained at the condition $|Q|/|S| = |P|/|S|$. Thus, separator thickness, i.e. molar conductivity of the electrolyte inside the separator matrix have noticeable influence on τ_R.

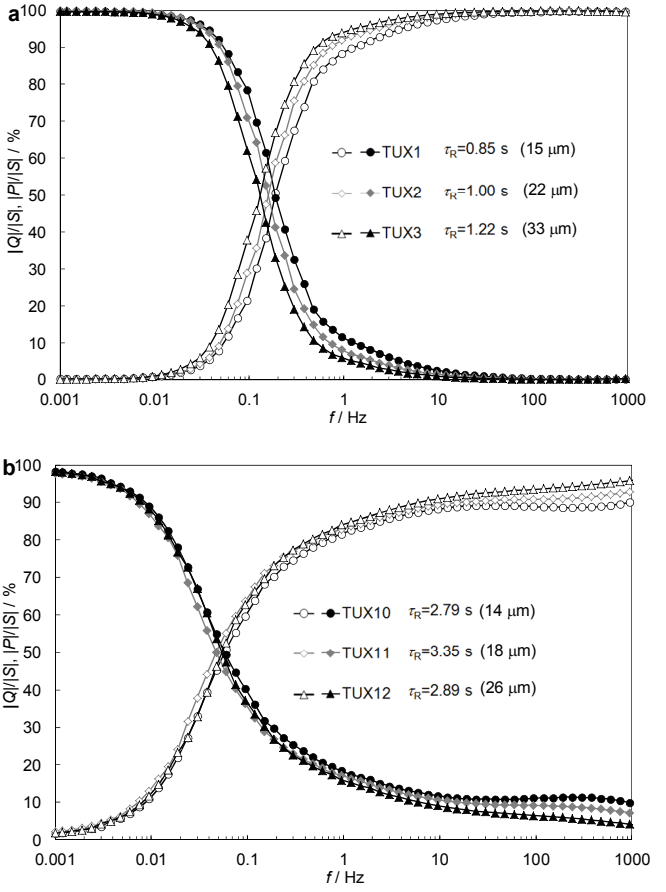

Figure 24. Normalized reactive power $|Q|/|S|$ (filled marks) and active power $|P|/|S|$ (open marks) vs. *ac* frequency plots for EDLCs completed using separators of different thicknesses (noted in figures) in: a) 1 M $TEMABF_4$ + AN at 3.0 V and b) $EMImBF_4$ at 3.2 V.

6.2.3. Constant power discharge test results

The specific energy vs. power relationship has been obtained from constant power discharge tests within the cell voltage range from 3.0 V to 1.5 V (Fig. 25). The Ragone plots for different EDLCs at moderate power densities

noticeably depend on the separator thickness, i.e. on the molar conductivity of the electrolyte in the separator matrix. EDLCs based on thinner separators deliver higher power at constant energy.

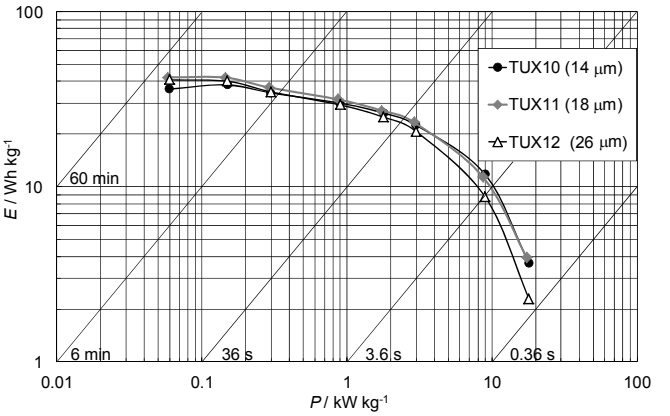

Figure 25. Ragone plots for EDLCs completed using separators of different thicknesses (noted in figure) in $EMImBF_4$.

6.3. Influence of temperature on the electrochemical behaviour of EDLCs [IV]

To study the influence of separator material parameters and temperature on the performance of EDLCs, 4 different separator materials (2 commercial and 2 self-made ones) were tested at lower temperatures in 1 M $TEMABF_4$ + (DMF+EC+PC) solution. All electrochemical measurements were carried out at fixed temperatures +24, +10, –10, and –30 °C. For evaluating the influence of temperature on the components thermal stability and performance of EDLC, the EDLCs were measured twice at +24 ° C, thus, before and after low temperature measurements.

6.3.1. Cyclic voltammetry data

Figure 26 shows that j depends nearly linearly on the cell voltage, except at the temperature –30 °C and at $U \geq 2.0$ V, where the influence of the ohmic resistance and slow mass transfer steps are noticeable.

The cyclic voltammograms measured are symmetrical with respect to the zero current line and have a nearly rectangular shape. The capacitance vs. U plots (Figs. 27a–27c) show that the nearly ideal capacitive behavior has been established at cell voltage scan rates $v \leq 20\ \mathrm{mV\ s^{-1}}$ and at cell potential $U \leq 3.2$ V

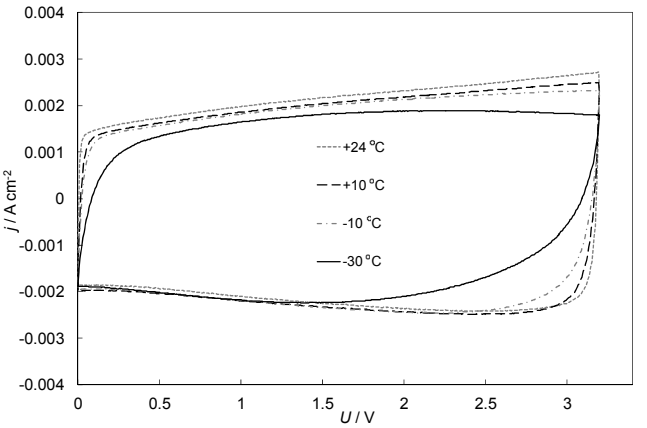

Figure 26. Current density vs. cell voltage curves for TUX10 separator based EDLCs at scan rate of 5 mV s^{-1} at different temperatures (noted in figure).

Also the nearly ideal capacitive behavior of EDLCs at temperature –10 °C has been established at cell voltage scan rates $v \leq 5$ mV s^{-1} and $U \leq 3.2$ V (Fig. 27b). However, at –30 °C (Fig. 27c), the nearly ideal capacitive behavior can be seen only at potential scan rates $v \leq 5$ mV s^{-1} for TUX10 separator based system. At voltage scan rates $v \leq 2$ mV s^{-1} and $U \leq 3.0$ V noticeable deviations have been established for other separators based EDLCs.

6.3.2. Electrochemical impedance spectroscopy data

According to the data in Figures 28a–28c, $R_s(\omega \to \infty)$ increases in the order of separators: TUX10 < TF4425 < Celgard2400 < TUX5 at any temperature investigated. Separator materials with higher porosity (TUX10, TF4425) have smaller high-frequency series resistance than materials with lower porosity (Celgard2400, TUX5). For Celgard2400 and TUX5 separator based EDLCs, the depressed semicircle can be seen in the region of high and medium *ac* frequency ($1.7 < f < 300\,000$ Hz) within the temperature range from +24 °C to –30 °C. Thus, the high-frequency behavior of EDLC is influenced by the electrolyte resistance in the more compact separator materials under study. However, this semicircle can be seen for all the EDLC systems at temperature –30 °C (Fig. 28c). From the Fig. 29, it can be seen, that high-frequency equivalent series resistance values for TUX10 separator based EDLC increase approximately 1.7 and 5 times, when the temperature decreases from +24 °C to –10 °C or to –30 °C, respectively, which could be explained by the lower mass transfer rate of the ions in micromesoporous carbon electrodes and porous separator matrix used.

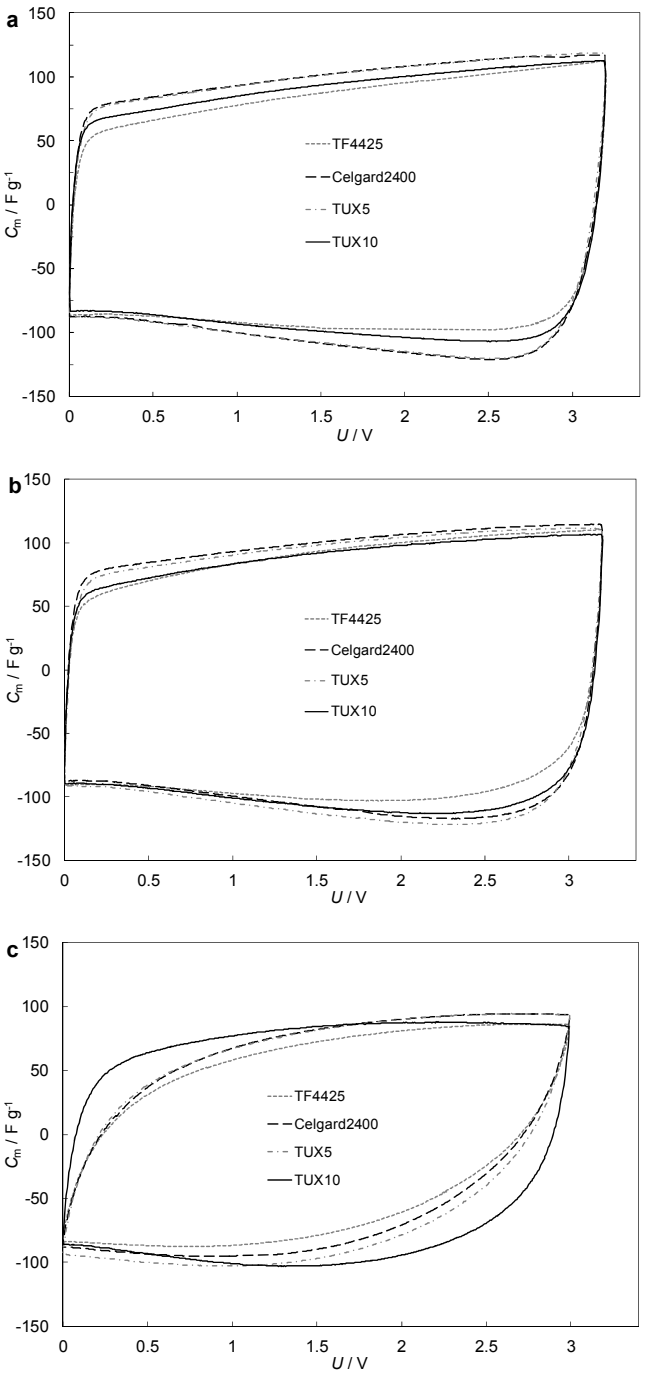

Figure 27. Specific capacitance vs. cell voltage curves for the EDLC cells based on different separator materials in 1 M $TEMABF_4$ + (DMC+EC+PC) electrolyte at temperatures: a) +24 °C and at scan rate of 20 mV s^{-1}, b) –10 °C, and c) –30 °C at scan rate 5 mV s^{-1}.

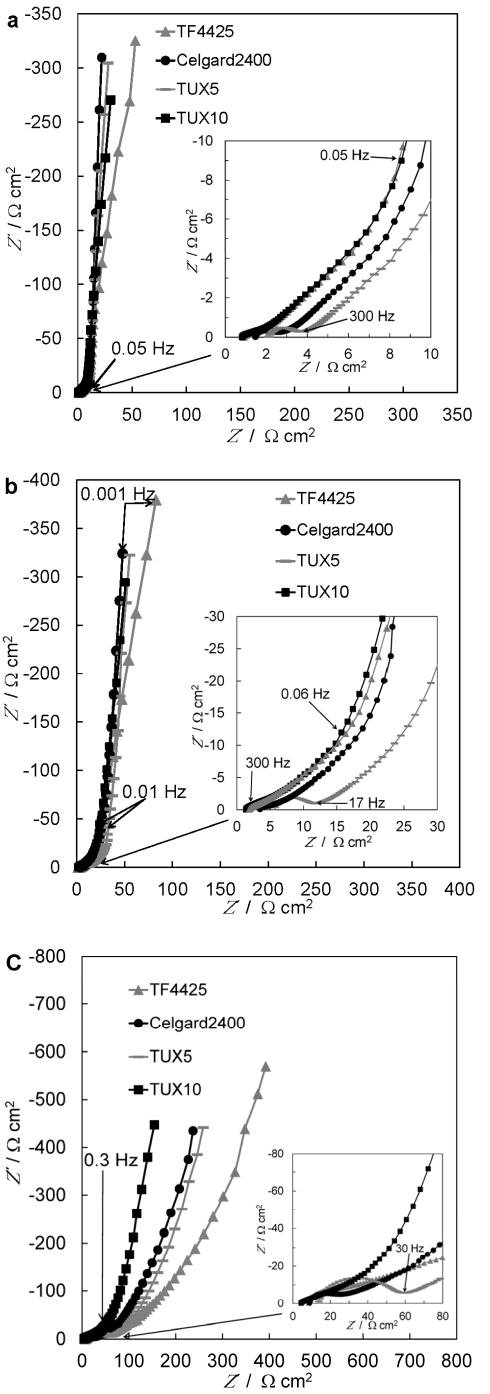

Figure 28. Nyquist plots for the EDLC cells completed using different separator materials (noted in figures) in 1 M $TEMABF_4$ + (DMC+EC+PC) solution at cell voltage 3.2 V and at temperatures: a) +24 °C, b) –10, and c) –30 °C.

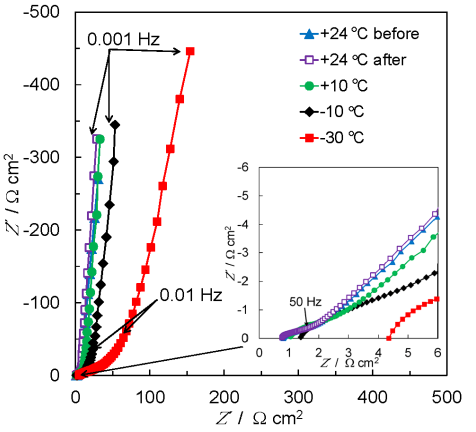

Figure 29. Nyquist plots for the EDLC cell completed using TUX10 separator material in 1 M $TEMABF_4$ + (DMC+EC+PC) solution at cell voltage 3.2 V and at different temperatures (noted in figure).

According to the phase angle vs. *ac* frequency relationship (Fig. 30) the nearly ideal capacitive behavior has been established at room temperature (Fig. 30). However, at –30 °C, it can be seen, that EDLCs completed with TF4425, TUX5 and Celgard2400 separators have much lower phase angle values than EDLC with TUX10 separator, explained by the lower resistance for TUX10 than that for other separators.

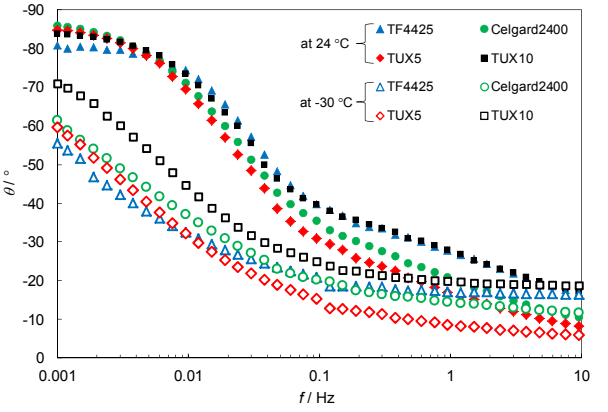

Figure 30. Phase angle vs. *ac* frequency plots at cell voltage 3.2 V for the EDLC cells completed using different separator materials (noted in figure) in 1 M $TEMABF_4$ + (DMC+EC+PC) electrolyte at temperatures +24 °C (filled marks) and –30 °C (open marks).

From Figure 31, it can be seen, that the absolute values of phase angle start to decrease noticeably at $T \leq -10$ °C, causing the deviation of EDLCs from the ideal capacitive behavior.

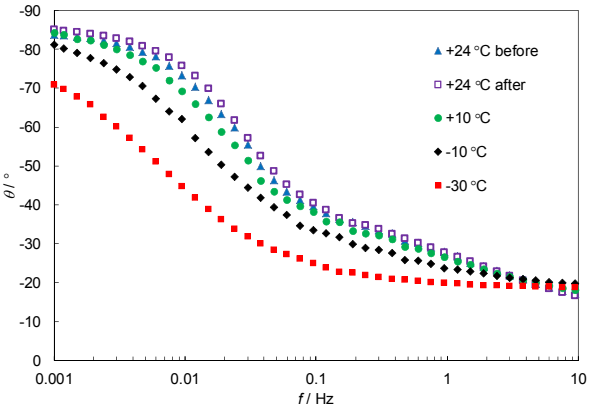

Figure 31. Phase angle vs. *ac* frequency plots at cell voltage 3.2 V for the EDLC cell completed using TUX10 separator material in 1 M $TEMABF_4$ + (DMC+EC+PC) electrolyte at different temperatures (noted in figure).

The series capacitance ($C_s(\omega \rightarrow 0)$) values (Fig. 32), calculated from impedance data, are in a good agreement with the values of C_m obtained using CV method at $v \leq 5$ mV s^{-1} (Fig. 27). At lower temperatures the characteristic time constant increases and C_s (Fig. 32) decreases noticeably because of the lower mass transfer rate of the electrolyte ions in the micromesoporous carbon electrodes. At $U = 3.2$ V, the C_s values are nearly independent of T, only if $T \geq +10$ °C. These data show, that at $T = -30$ °C, the adsorption equilibrium has not been established even at *ac* frequency $f \geq 1 \times 10^{-3}$ Hz. Thus, in the medium and low *ac* frequency region, C_s strongly depends on the temperature applied, demonstrating that the characteristic time constant of EDLCs increases with the decrease in temperature.

The dependence of the C_p/C_s ratio on frequency is shown in Figure 33 and for the ideally polarizable system, the ratio $C_p/C_s = 1$, which can be seen for all EDLCs under study at room temperature. At lower temperatures $T \leq +10$ °C, the C_p/C_s ratio starts to decrease, indicating to the slow mass transfer rate of the ions inside the porous electrode matrix.

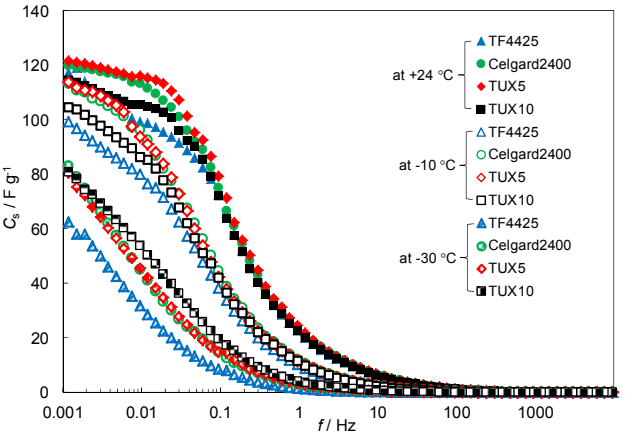

Figure 32. Specific series capacitance C_s vs. *ac* frequency dependencies at cell voltage 3.2 V for the EDLC cells completed using different separator materials (noted in figure) in 1 M $TEMABF_4$ + (DMC+EC+PC) electrolyte at different temperatures (noted in figure).

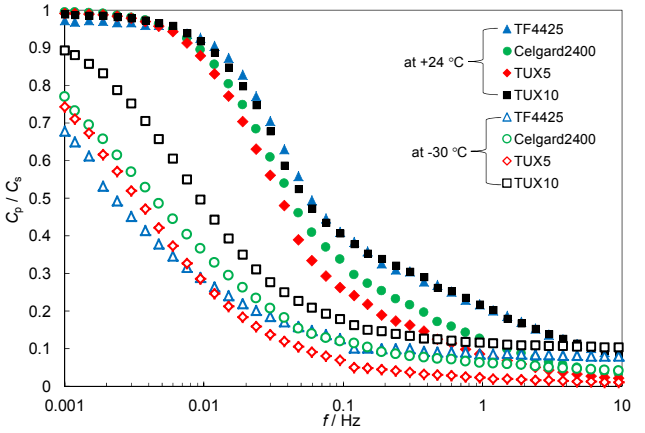

Figure 33. C_p/C_s ratio vs. *ac* frequency dependencies at cell voltage 3.2 V for the EDLC cells completed using different separator materials (noted in figure) in 1 M $TEMABF_4$ + (DMC+EC+PC) electrolyte at temperature +24 °C (filled marks) and –30 °C (open marks).

The relaxation time constant (τ_R) values, are presented in the Table VII. τ_R clearly depends on the temperature and separator material used. The calculated values of τ_R noticeably increase with lowering the temperature (τ_R = 2.98 s at +24 °C and τ_R = 17.1 s at –30 °C, Table VII). A comparison between self-made separator TUX10 and commercial separator TF4425 shows that at –30 °C the TUX10 based EDLC is able to deliver the stored energy ~4 times faster than the EDLC completed with commercial separator. At T = +24 °C, this difference is

only ~1.5 times. Thus, separator porosity and molar conductivity of the electrolyte in the porous separator matrix have noticeable influence on the characteristic time constant values, especially at lower temperatures.

Table VII. Characteristic time constant (τ_R) values calculated from impedance data at the condition $|Q|/|S| = |P|/|S|$.

Temperature / Separator	+24 °C before	+10 °C	–10 °C	–30 °C	+24 °C after
TF4425	2.70 s	3.50 s	5.24 s	69.5 s	2.53 s
Celgard2400	3.74 s	4.91 s	7.84 s	36.0 s	3.54 s
TUX5	4.44 s	5.77 s	12.2 s	48.2 s	4.47 s
TUX10	2.98 s	3.77 s	5.56 s	17.1 s	2.60 s

6.3.3. Maximum specific energy and power values for EDLCs based on different separators and electrolytes

It was found that the specific energy weakly depends on the separator material parameters, if $T \geq -10$ °C (Fig. 34). Thus, at $T \geq -10$ °C, the E_{max} value for fully charged/discharged system is determined mainly by the microporous TiC-CDC electrode material properties and temperature. At $T = -30$ °C, the E_{max} values are noticeably lower than that at $T = +24$ °C. However, the specific power depends noticeably on temperature and separator material parameters (porosity, thus on the conductivity of the electrolyte in the separator matrix) being highest for TUX10 based EDLC (Fig. 34). At –30 °C, P_{max} is approximately 5 times lower than that at +24 °C for TUX10 based EDLC, but P_{max} value decreases approximately 9 times for TF4425 based EDLC, when the temperature changes from +24 °C to –30 °C.

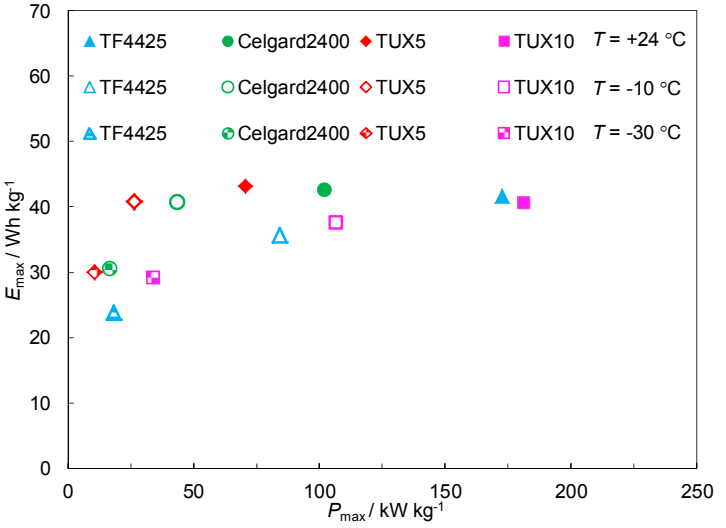

Figure 34. Maximum specific energy (E_{max}) vs. specific power (P_{max}) plots at cell voltage 3.2 V for the EDLC cells completed using different separator materials (noted in figure) in 1 M $TEMABF_4$+(DMC+EC+PC) electrolyte at temperature +24 °C (filled marks), –10 °C (open marks), and –30 °C (pattern marks).

7. SUMMARY

Electrospinning method has been used for the preparation of different poly(vinylidene fluoride) (PVDF) polymer membranes. Electrospinning parameters were varied to prepare different PVDF membranes with various morphologies, porosities, surface areas, pore size distributions and thicknesses. The parameters for self-made separators have been compared with these for commercial separators TF4425 and Celgard2400.

Influence of the separator characteristics (chemical composition, morphology, total porosity and thickness) on the parameters of the electrical double-layer capacitor (EDLC) cell, based on two ideally polarizable microporous titanium carbide-derived carbon (TiC-CDC) electrodes and different electrolytes (1 M triethylmethylammonium tetrafluoroborate in acetonitrile; 1 M triethylmethylammonium tetrafluoroborate in dimethyl carbonate, ethylene carbonate and propylene carbonate mixture with 1:1:1 volume ratio; and room temperature ionic liquid 1-ethyl-3-methylimidazolium tetrafluoroborate), have been tested by cyclic voltammetry, electrochemical impedance spectroscopy, and constant power discharge methods.

The limits of ideal polarizability, low-frequency limiting series capacitance and resistance, parallel capacitance and resistance, characteristic relaxation time constant, complex power components and specific energy and power values, dependent on the polymer separator characteristics, have been obtained and discussed.

It was found that at low voltage scan rates the separator materials characteristics have a little influence on the shape of the cyclic voltammetry curves, and EDLCs charging/discharging current and capacitance are mainly determined by the properties of the electrode material. It was found from the impedance data that the high frequency series resistance, phase angle, low and medium frequency series and parallel resistance, characteristic relaxation time constant and specific power values of EDLC noticeably depend on the parameters of the separator used, i.e. on the chemical composition, surface morphology, total porosity and thickness of the membrane used in EDLC.

Thus, for the high power pulse generation systems, the properties of the separator material have to be carefully optimized. This effect seems to be highly important for the EDLCs based on more viscous (including room temperature ionic liquid) electrolytes, and for the electrochemical systems working at lower temperatures.

8. REFERENCES

[1] A. Formhals. US Patent Patent 1,975,504, 1934.
[2] A. Formhals. US Patent Patent 2,160,962, 1939.
[3] A. Formhals. US Patent Patent 2,187,306, 1940.
[4] S. Ramakrishna, K. Fujihara, W.-E. Teo, T.-C. Lim, Z. Ma, An Introduction to Electrospinning and Nanofibers, World Scientific Publishing Co. Pte. Ltd., Singapore 2005.
[5] A. L. Andrady, Science and technology of polymer nanofibers, John Wiley & Sons, Inc., New Jersey 2008.
[6] S. J. Doh, C. Kim, S. G. Lee, S. J. Lee, H. Kim, Journal of Hazardous Materials 154 (2008) 118–127.
[7] Z.-M. Huang, Y.-Z. Zhang, M. Kotaki, S. Ramakrishna, Composites Science and Technology 63 (2003) 223–2253.
[8] L. Dan, X. Younan, Advanced Materials 16 (2004)1151–1170.
[9] J. M. Deitzel, J. Kleinmeyer, D. Harris, N. C. Beck Tan, Polymer 42 (2000) 261–272.
[10] H. Fong, I. Chun, D. H. Reneker, Polymer 40 (1999) 4585–4592.
[11] T. J. Sill, H. A. von Recum, Biomaterials 29 (2008) 1989–2006.
[12] W. E. Teo, S. Ramakrishna, Nanotechnology 17 (2006) R89–R106.
[13] S. L. Shenoy, W. D. Bates, H. L. Frisch, G. E. Wnek, Polymer 46 (2005) 3372–3384.
[14] T. Jarusuwannapoom, W. Hongrojjanawiwat, S. Jitjaicham, L. Wannatong, M. Nithitanakul, C. Pattamaprom, P. Koombhongse, R. Rangkupan, P. Supaphol, Euro. Polym. J. 41 (2005) 409–421.
[15] L. Wannatong, A. Sirivat, P. Supaphol, Polymer International 53 (2004) 1851–1859.
[16] X. Zong, K. Kim, D. Fang, S. Ran, B. S. Hsiao, B. Chu, Polymer 43 (2002) 4403–4412.
[17] X. Mo, C. Xu, M. Kotaki, S. Ramakrishna, Biomaterials 25 (2004)1883–1890.
[18] C. J. Buchko, C. L. Chen, Y. Shen, D. C. Martin, Polymer 40 (1999) 7397–7407.
[19] K. W. Kim, K. H. Lee, M. S. Khil, Y. S. Ho, H. Y. Kim, Fibers and Polymers 5 (2004) 122–127.
[20] F.-L. Zhou, R.-H. Gong, Polymer International 57 (2008) 837–845.
[21] S. Thandavamoorthy, G. S. Bhat, R. W. Tock, S. Parameswaran, S. S. Ramkumar, J. Appl. Polym. Sci. 96 (2005) 557–569.
[22] S. J. Doh, C. Kim, S. G. Lee, S. J. Lee, H. Kim, Journal of Hazardous Materials 154 (2008) 118–127.
[23] K. Tõnurist, A. Jänes, T. Thomberg, H. Kurig, E. Lust, J. Electrochem. Soc. 156 (2009) A334–A342.
[24] K. Tõnurist, T. Thomberg, A. Jänes, I. Kink, E. Lust, Electrochem. Commun. 22 (2012) 77–80.
[25] K. Tõnurist, T. Thomberg, A. Jänes, T. Romann, V. Sammelselg, E. Lust, J. Electroanal. Chem. 689 (2013) 8–20.
[26] K. Tõnurist, T. Thomberg, A. Jänes, E. Lust, J. Electrochem. Soc. 160 (2013) A449–A457.
[27] K. Tõnurist, T. Thomberg, A. Jänes, E. Lust, ECS Trans. 50 (2013) 49–58.
[28] K. Tõnurist, T. Thomberg, A. Jänes, E. Lust, ECS Trans. 50 (2013) 181–189.
[29] B. E. Conway, Electrochemical Supercapacitors, Scientific Fundamentals and Technological Applications, Kluwer Acaemic / Plenum Publishers, New York 1999.

[30] R. Kötz, M. Carlen, Electrochimica Acta 45 (2000) 2483–2498.
[31] A. G. Pandolfo, A. F. Hollenkamp, J. Power Sources 157 (2006) 11–27.
[32] M. Winter, R. J. Brodd, Chemical Reviews 104 (2004) 4245–4269.
[33] A. Lewandowski, M. Galinki, J. Power Sources 173 (2007) 822–828.
[34] P. L Taberna, P. Simon and J. F. Fauvarque, J. Electrochem. Soc. 150 (2003) A292–A300.
[35] J. R. Miller, P. Simon, Science 321(2008) 651–652.
[36] J. R. Miller, A. F. Burk, The Electrochemical Society Inerface, Spring (2008) 53–57.
[37] P. Simon, Y. Gogotsi, Nature Materials 7 (2008) 845–854.
[38] P. Simon, A. Burke, The Electrochm. Soc. Inerface 1 (2008) 38–43.
[39] S. Lowell, J. E. Scields, M. A. Thomas, M. Thommes, Mercury Porosimetry: Non-wettin Liquid Penetration, Characterization of Porous Solids and Powders: Surface Area, Pore Size and Density, Kluwer Academic Publishers, Dordrecht 2004 p. 157–212.
[40] D. M. Smith, D. L. Stermer, Powder Technology 53 (1987) 23–30.
[41] R. Pospech, P. Schneider, Powder Technology 59 (1989) 163–17.
[42] V. Karageorgiou, D. Kaplan, Biomaterials 26 (2005) 5474–5491.
[43] P. Sharma, T. S. Bhatti, Energy Conversion and Managemen 51 (2010) 2901–2912.
[44] F. Beguin, E. Frackowiak, Carbons for Electrochemical Energy Storage and Conversion Systems, CRC Press, New York 2010.
[45] Y. Gogotsi, Nanomaterials Handbook, CRC Taylor & Francis, Florida 2006.
[46] O. Ioannidou, A. Zabaniotou, Renewable and Sustainable Energy Reviews 11 (2007) 966–2005.
[47] M. Inagaki, H. Konno, O. Tanaike, J. Power Sources 195 (2010) 7880–7903.
[48] P. Simon, Y. Gogotsi, Philosophical Transactions of the Royal Society A 368 (2010) 3457–3467.
[49] I. Tallo, T. Thomberg, H. Kurig, A. Jänes, K. Kontturi, E. Lust, J. Solid State Electrochem. 17 (2013) 19–28.
[50] I. Tallo, T. Thomberg, H. Kurig, A. Jänes, K. Kontturi, E. Lust, Carbon 49 (2011) 4427–4433.
[51] T. Thomber, H. Kurig, A. Jänes, E. Lust, Microporous and Mesoporous Materials 141 (2011) 88–93.
[52] A. Jänes, T. Thomber, E. Lust, Carbon 45 (2007) 2717–2722.
[53] S. S. Zhang, J. Power Sources 164 (2007) 351–364.
[54] H. Kurig, A. Jänes, E. Lust, J. Electrochem. Soc. 157 (2010) A272–A279.
[55] H. Kurig, A. Jänes, E. Lust, J. Mater. Res. 25 (2010) 1447–1450.
[56] A. Jänes, H. Kurig, T. Romann, E. Lust, Electrochem. Commun. 12 (2010) 535–539.
[57] E. Lust, A. Jänes, M. Arulepp, J. Electroanal. Chem. 562 (2004) 33–42.
[58] A. Jänes, E. Lust, J. Electroanal. Chem. 588 (2006) 285–295.
[59] E. Lust, A. Jänes, M. Arulepp, J. Solid State Electrochem. 8 (2004) 488–496.
[60] R. Palm, H. Kurig, K. Tonurist, A. Jänes, E. Lust, Electrochim. Acta 85 (2012) 139–144.
[61] E. Barsoukov, J. R. Mcdonald, Impedance spectroscopy. Theory, Experiment and Applications, 2nd ed, Wiley-Interscience, New Jersey (2005).
[62] M. Eikerling, A. A. Kornyshev, E. Lust, J. Electrochem. Soc. 152 (2005) E24–E33.

9. SUMMARY IN ESTONIAN

Elektroformeerimise meetodil valmistatud separaatormaterjalide mõju elektrilise kaksikkihi kondensaatori karakteristikutele

Antud töös kasutati elektroformeerimise meetodit polüvinülideenfluoriidist (PVDF) membraanide valmistamiseks. Varieerides elektroformeerimise parameetreid saadi erineva pinnamorfoloogia, poorsuse, eripinna, poorijaotuse ning paksusega PVDF membraanid, mille omadusi võrreldi kommertsiaalsete separaatorite TF4425 ja Celgard2400 karakteristikutega.

Uuriti separaatormaterjali parameetrite (keemiline koostis, morfoloogia, poorsus ja paksus) mõju elektrilise kaksikkihi kondensaatori (EKKK) karakteristikutele. Uuritavad EKKKd koosnesid kahest identsest titaankarbiidist sünteesitud ideaalselt polariseeritavast süsinikelektroodist ja erinevatest elektrolüütidest (1 M trietüülmetüülamoonium-tertafluoroboraat atsetoonitriilis; 1 M trietüülmetüülamoonium-tertafluoroboraat dimetüül- karbonaadi, etüleenkarbonaadi ja propüleenkarbonaadi 1:1:1 ruumala suhtega segus ja ioonne vedelik 1-etüül-3-metüül-imidasoolium-tetrafluoroboraat). Uuritavaid süsteeme uuriti tsüklilise voltamperomeetria, elektrokeemilise impedantsspektroskoopia ja konstantsel võimsusel tühjaks laadimise meetoditega.

Uuriti kuidas separaatormaterjali erinevad parameetrid mõjutavad EKKK ideaalse polariseeritavuse ala laiust, madalsageduslikku järjestikmahtuvust ning -takistust, paralleelmahtuvust ning -takistust, karakteristlikku ajakonstanti, kompleksvõimsuse komponente ning energia- ja võimsustihedust. Leiti, et separaatormaterjali karakteristikud mõjutavad vähesel määral tsükliliste voltamperogrammide kuju madalatel laotuskiirustel ning EKKK laadimise ja tühjenemise vool ning mahtuvus on põhiliselt ära määratud süsinikelektroodi materjali omadustega. Elektrokeemilise impedants-spektroskoopia mõõtmistulemustest leiti, et separaatormaterjali karakteristikud nagu keemiline koostis, pinna morfoloogia, poorsus, ja paksus mõjutavad oluliselt kõrgsageduslikku järjestiktakistust, faasinurka, madal- ja kesksageduslikku järjestik- ning paralleltakistust, karakteristlikku ajakonstanti ning võimsustihedust.

Seega tuleb kõrge energia- ja võimsustihedusega EKKK valmistamiseks separaatormaterjalide karakteristikud hoolikalt optimeerida. Separaatori mõju EKKK karakteristikutele on eriti oluline suurema viskoossusega elektrolüütide korral (toatemperatuuril ioonsed vedelikud) ning teistes elektrokeemilistes süsteemides, mis töötavad madalamatel temperatuuridel.

10. ACKNOWLEDGEMENTS

First and foremost, I would like to express my greatest gratitude to my supervisors professor Enn Lust, and Dr. Thomas Thomberg for their patience, guidance and support during all these years of our collaboration.

Many thanks go to my colleagues for encouragement, I am grateful for all of these inspiring discussions over the years.

Last but not least, I would like to thank my family and friends for supporting me all the time.

This research is financially supported by Estonian Science Foundation (grants no. 8172 and 8786), Estonian Ministry of Education and Research (project SF0180002s08), graduate school 'Functional materials and processes' (European Social Fund project 1.2.0401.09–0079), European Regional Development Fund: Estonian Materials Technology project (3.2.1101.12–0019), Estonian Centres of Excellence in Research project (3.2.0101–0030), and Estonian Energy Technology project (3.2.0501.10–0015).

11. PUBLICATIONS

CURRICULUM VITAE

Name: Kerli Tõnurist
Date of birth: January 18, 1985
Citizenship: Estonian
Contact: Institute of Chemistry, University of Tartu
Ravila 14a, 50411 Tartu, Estonia
E-mail: kerli123@hotmail.com

Education:

2009–…	University of Tartu, Institute of Chemistry, PhD student
2007–2009	University of Tartu – Master's degree in electrochemistry (*cum laude*)
2004–2007	University of Tartu – Bachelor degree in chemistry

Professional employment:

2009–…	University of Tartu, Institute of Chemistry, Chemist
2006–2009	University of Tartu, Institute of Chemistry, Laboratorian

List of Publications:

1. A. Jänes, T. Thomberg, K. Tõnurist, H. Kurig, A. Laheäär, E. Lust, Micro- and Mesoporous Carbide-Derived Carbon Materials and Polymer Membranes for Supercapacitors. ECS Trans., 1 (2008) 57–67
2. K. Tõnurist, A. Jänes, T. Thomberg, H. Kurig, E. Lust, Influence of Mesoporous Separator Properties on the Parameters of Electrical Double-Layer Capacitor Single Cells. J. Electrochem. Soc., 156 (2009) A334–A342.
3. A. Jänes, K. Tõnurist, T. Thomberg, E. Lust, Comparison of Electrospun and Commercially Available Separator Materials for Supercapacitors. ECS Trans., 30 (2009) 23–32.
4. K. Tõnurist, T. Thomberg, A. Jänes, I. Kink, E. Lust, Specific Performance of Electrical Double Layer Capacitors Based on Different Separator Materials in Room Temperature Ionic Liquid. Electrochem. Commun., 22 (2012) 77 – 80.
5. R. Palm, H. Kurig, K. Tõnurist, A. Jänes, E. Lust, Is the Mixture of 1-Ethyl-3-Methylimidazolium Tetrafluoroborate and 1-Butyl-3-Methylimidazolium Tetrafluoroborate Applicable as Electrolyte in Electrical Double Layer Capacitors?. Electrochem. Commun., 22 (2012) 203–206.
6. R. Palm, H. Kurig, K. Tõnurist, A. Jänes, E. Lust, Electrical Double Layer Capacitors Based on 1-Ethyl-3-Methylimidazolium Tetrafluoroborate With Small Addition of Acetonitrile. Electrochimica Acta, 85 (2012) 139–144.
7. K. Tõnurist, T. Thomberg, A. Jänes, T. Romann, V. Sammelselg, E. Lust, Influence of Separator Properties on Electrochemical Performance of Electrical Double–Layer Capacitors. J. Electroanal. Chem., 689 (2013) 8–20.

8. K. Tõnurist, T. Thomberg, A. Jänes, E. Lust, Specific Performance of Supercapacitors at Low Temperatures Based on Different Separator Materials. J. Electrochem. Soc., 160 (2013) A449–A457.
9. K. Tõnurist, T. Thomberg, A. Jänes, E. Lust, Specific Performance of Electrical Double–Layer Capacitors Based on Different Separator Materials and Non–Aqueous Electrolytes. ECS Trans., 50 (2013) 181–189.
10. K. Tõnurist, T. Thomberg, A. Jänes, T. Romann, V. Sammelselg, E. Lust, Polymorphic Behavior and Morphology of Electrospun Poly(vinylidene Fluoride) Separator Materials for Non-Aqueous Electrolyte Based Electric Double Layer Capacitors. ECS Trans., 50 (2013) 49–58.

ELULOOKIRJELDUS

Nimi: Kerli Tõnurist
Sünniaeg: 18. jaanuar 1985
Kodakondsus: Eesti
Kontakt: Keemia Instituut, Tartu Ülikool
Ravila 14a, 50411 Tartu, Eesti
E-post: kerli123@hotmail.com

Haridus:

2009–…	Tartu Ülikool, Keemia Instituut, doktorant
2007–2009	Tartu Ülikool – Magistrikraad elektrokeemias (*cum laude*)
2004–2007	Tartu Ülikool – Bakalaureusekraad keemias

Teenistuskäik:

2009–…	Tartu Ülikool, Keemia Instituut, keemik
2006–2008	Tartu Ülikool, Keemia Instituut, laborant

Teaduspublikatsioonid

1. A. Jänes, T. Thomberg, K. Tõnurist, H. Kurig, A. Laheäär, E. Lust, Micro- and Mesoporous Carbide-Derived Carbon Materials and Polymer Membranes for Supercapacitors. ECS Trans., 1 (2008) 57–67
2. K. Tõnurist, A. Jänes, T. Thomberg, H. Kurig, E. Lust, Influence of Mesoporous Separator Properties on the Parameters of Electrical Double-Layer Capacitor Single Cells. J. Electrochem. Soc., 156 (2009) A334–A342.
3. A. Jänes, K. Tõnurist, T. Thomberg, E. Lust, Comparison of Electrospun and Commercially Available Separator Materials for Supercapacitors. ECS Trans., 30 (2009) 23–32.
4. K. Tõnurist, T. Thomberg, A. Jänes, I. Kink, E. Lust, Specific Performance of Electrical Double Layer Capacitors Based on Different Separator Materials in Room Temperature Ionic Liquid. Electrochem. Commun., 22 (2012) 77 – 80.
5. R. Palm, H. Kurig, K. Tõnurist, A. Jänes, E. Lust, Is the Mixture of 1-Ethyl-3-Methylimidazolium Tetrafluoroborate and 1-Butyl-3-Methylimidazolium Tetrafluoroborate Applicable as Electrolyte in Electrical Double Layer Capacitors?. Electrochem. Commun., 22 (2012) 203–206.
6. R. Palm, H. Kurig, K. Tõnurist, A. Jänes, E. Lust, Electrical Double Layer Capacitors Based on 1-Ethyl-3-Methylimidazolium Tetrafluoroborate With Small Addition of Acetonitrile. Electrochimica Acta, 85 (2012) 139–144.
7. K. Tõnurist, T. Thomberg, A. Jänes, T. Romann, V. Sammelselg, E. Lust, Influence of Separator Properties on Electrochemical Performance of Electrical Double–Layer Capacitors. J. Electroanal. Chem., 689 (2013) 8–20.

8. K. Tõnurist, T. Thomberg, A. Jänes, E. Lust, Specific Performance of Supercapacitors at Low Temperatures Based on Different Separator Materials. J. Electrochem. Soc., 160 (2013) A449–A457.
9. K. Tõnurist, T. Thomberg, A. Jänes, E. Lust, Specific Performance of Electrical Double–Layer Capacitors Based on Different Separator Materials and Non–Aqueous Electrolytes. ECS Trans., 50 (2013) 181–189.
10. K. Tõnurist, T. Thomberg, A. Jänes, T. Romann, V. Sammelselg, E. Lust, Polymorphic Behavior and Morphology of Electrospun Poly(vinylidene Fluoride) Separator Materials for Non-Aqueous Electrolyte Based Electric Double Layer Capacitors. ECS Trans., 50 (2013) 49–58.

DISSERTATIONES CHIMICAE UNIVERSITATIS TARTUENSIS

1. **Toomas Tamm.** Quantum-chemical simulation of solvent effects. Tartu, 1993, 110 p.
2. **Peeter Burk.** Theoretical study of gas-phase acid-base equilibria. Tartu, 1994, 96 p.
3. **Victor Lobanov.** Quantitative structure-property relationships in large descriptor spaces. Tartu, 1995, 135 p.
4. **Vahur Mäemets.** The ^{17}O and ^{1}H nuclear magnetic resonance study of H_2O in individual solvents and its charged clusters in aqueous solutions of electrolytes. Tartu, 1997, 140 p.
5. **Andrus Metsala.** Microcanonical rate constant in nonequilibrium distribution of vibrational energy and in restricted intramolecular vibrational energy redistribution on the basis of slater's theory of unimolecular reactions. Tartu, 1997, 150 p.
6. **Uko Maran.** Quantum-mechanical study of potential energy surfaces in different environments. Tartu, 1997, 137 p.
7. **Alar Jänes.** Adsorption of organic compounds on antimony, bismuth and cadmium electrodes. Tartu, 1998, 219 p.
8. **Kaido Tammeveski.** Oxygen electroreduction on thin platinum films and the electrochemical detection of superoxide anion. Tartu, 1998, 139 p.
9. **Ivo Leito.** Studies of Brønsted acid-base equilibria in water and non-aqueous media. Tartu, 1998, 101 p.
10. **Jaan Leis.** Conformational dynamics and equilibria in amides. Tartu, 1998, 131 p.
11. **Toonika Rinken.** The modelling of amperometric biosensors based on oxidoreductases. Tartu, 2000, 108 p.
12. **Dmitri Panov.** Partially solvated Grignard reagents. Tartu, 2000, 64 p.
13. **Kaja Orupõld.** Treatment and analysis of phenolic wastewater with microorganisms. Tartu, 2000, 123 p.
14. **Jüri Ivask.** Ion Chromatographic determination of major anions and cations in polar ice core. Tartu, 2000, 85 p.
15. **Lauri Vares.** Stereoselective Synthesis of Tetrahydrofuran and Tetrahydropyran Derivatives by Use of Asymmetric Horner-Wadsworth-Emmons and Ring Closure Reactions. Tartu, 2000, 184 p.
16. **Martin Lepiku.** Kinetic aspects of dopamine D_2 receptor interactions with specific ligands. Tartu, 2000, 81 p.
17. **Katrin Sak.** Some aspects of ligand specificity of P2Y receptors. Tartu, 2000, 106 p.
18. **Vello Pällin.** The role of solvation in the formation of iotsitch complexes. Tartu, 2001, 95 p.

19. **Katrin Kollist.** Interactions between polycyclic aromatic compounds and humic substances. Tartu, 2001, 93 p.
20. **Ivar Koppel.** Quantum chemical study of acidity of strong and superstrong Brønsted acids. Tartu, 2001, 104 p.
21. **Viljar Pihl.** The study of the substituent and solvent effects on the acidity of OH and CH acids. Tartu, 2001, 132 p.
22. **Natalia Palm.** Specification of the minimum, sufficient and significant set of descriptors for general description of solvent effects. Tartu, 2001, 134 p.
23. **Sulev Sild.** QSPR/QSAR approaches for complex molecular systems. Tartu, 2001, 134 p.
24. **Ruslan Petrukhin.** Industrial applications of the quantitative structure-property relationships. Tartu, 2001, 162 p.
25. **Boris V. Rogovoy.** Synthesis of (benzotriazolyl)carboximidamides and their application in relations with *N*- and *S*-nucleophyles. Tartu, 2002, 84 p.
26. **Koit Herodes.** Solvent effects on UV-vis absorption spectra of some solvatochromic substances in binary solvent mixtures: the preferential solvation model. Tartu, 2002, 102 p.
27. **Anti Perkson.** Synthesis and characterisation of nanostructured carbon. Tartu, 2002, 152 p.
28. **Ivari Kaljurand.** Self-consistent acidity scales of neutral and cationic Brønsted acids in acetonitrile and tetrahydrofuran. Tartu, 2003, 108 p.
29. **Karmen Lust.** Adsorption of anions on bismuth single crystal electrodes. Tartu, 2003, 128 p.
30. **Mare Piirsalu.** Substituent, temperature and solvent effects on the alkaline hydrolysis of substituted phenyl and alkyl esters of benzoic acid. Tartu, 2003, 156 p.
31. **Meeri Sassian.** Reactions of partially solvated Grignard reagents. Tartu, 2003, 78 p.
32. **Tarmo Tamm.** Quantum chemical modelling of polypyrrole. Tartu, 2003. 100 p.
33. **Erik Teinemaa.** The environmental fate of the particulate matter and organic pollutants from an oil shale power plant. Tartu, 2003. 102 p.
34. **Jaana Tammiku-Taul.** Quantum chemical study of the properties of Grignard reagents. Tartu, 2003. 120 p.
35. **Andre Lomaka.** Biomedical applications of predictive computational chemistry. Tartu, 2003. 132 p.
36. **Kostyantyn Kirichenko.** Benzotriazole – Mediated Carbon–Carbon Bond Formation. Tartu, 2003. 132 p.
37. **Gunnar Nurk.** Adsorption kinetics of some organic compounds on bismuth single crystal electrodes. Tartu, 2003, 170 p.
38. **Mati Arulepp.** Electrochemical characteristics of porous carbon materials and electrical double layer capacitors. Tartu, 2003, 196 p.

39. **Dan Cornel Fara.** QSPR modeling of complexation and distribution of organic compounds. Tartu, 2004, 126 p.
40. **Riina Mahlapuu.** Signalling of galanin and amyloid precursor protein through adenylate cyclase. Tartu, 2004, 124 p.
41. **Mihkel Kerikmäe.** Some luminescent materials for dosimetric applications and physical research. Tartu, 2004, 143 p.
42. **Jaanus Kruusma.** Determination of some important trace metal ions in human blood. Tartu, 2004, 115 p.
43. **Urmas Johanson.** Investigations of the electrochemical properties of polypyrrole modified electrodes. Tartu, 2004, 91 p.
44. **Kaido Sillar.** Computational study of the acid sites in zeolite ZSM-5. Tartu, 2004, 80 p.
45. **Aldo Oras.** Kinetic aspects of dATPαS interaction with $P2Y_1$ receptor. Tartu, 2004, 75 p.
46. **Erik Mölder.** Measurement of the oxygen mass transfer through the air-water interface. Tartu, 2005, 73 p.
47. **Thomas Thomberg.** The kinetics of electroreduction of peroxodisulfate anion on cadmium (0001) single crystal electrode. Tartu, 2005, 95 p.
48. **Olavi Loog.** Aspects of condensations of carbonyl compounds and their imine analogues. Tartu, 2005, 83 p.
49. **Siim Salmar.** Effect of ultrasound on ester hydrolysis in aqueous ethanol. Tartu, 2006, 73 p.
50. **Ain Uustare.** Modulation of signal transduction of heptahelical receptors by other receptors and G proteins. Tartu, 2006, 121 p.
51. **Sergei Yurchenko.** Determination of some carcinogenic contaminants in food. Tartu, 2006, 143 p.
52. **Kaido Tämm.** QSPR modeling of some properties of organic compounds. Tartu, 2006, 67 p.
53. **Olga Tšubrik.** New methods in the synthesis of multisubstituted hydrazines. Tartu. 2006, 183 p.
54. **Lilli Sooväli.** Spectrophotometric measurements and their uncertainty in chemical analysis and dissociation constant measurements. Tartu, 2006, 125 p.
55. **Eve Koort.** Uncertainty estimation of potentiometrically measured ph and pK_a values. Tartu, 2006, 139 p.
56. **Sergei Kopanchuk.** Regulation of ligand binding to melanocortin receptor subtypes. Tartu, 2006, 119 p.
57. **Silvar Kallip.** Surface structure of some bismuth and antimony single crystal electrodes. Tartu, 2006, 107 p.
58. **Kristjan Saal.** Surface silanization and its application in biomolecule coupling. Tartu, 2006, 77 p.
59. **Tanel Tätte.** High viscosity $Sn(OBu)_4$ oligomeric concentrates and their applications in technology. Tartu, 2006, 91 p.

60. **Dimitar Atanasov Dobchev**. Robust QSAR methods for the prediction of properties from molecular structure. Tartu, 2006, 118 p.
61. **Hannes Hagu**. Impact of ultrasound on hydrophobic interactions in solutions. Tartu, 2007, 81 p.
62. **Rutha Jäger.** Electroreduction of peroxodisulfate anion on bismuth electrodes. Tartu, 2007, 142 p.
63. **Kaido Viht.** Immobilizable bisubstrate-analogue inhibitors of basophilic protein kinases: development and application in biosensors. Tartu, 2007, 88 p.
64. **Eva-Ingrid Rõõm.** Acid-base equilibria in nonpolar media. Tartu, 2007, 156 p.
65. **Sven Tamp.** DFT study of the cesium cation containing complexes relevant to the cesium cation binding by the humic acids. Tartu, 2007, 102 p.
66. **Jaak Nerut.** Electroreduction of hexacyanoferrate(III) anion on Cadmium (0001) single crystal electrode. Tartu, 2007, 180 p.
67. **Lauri Jalukse.** Measurement uncertainty estimation in amperometric dissolved oxygen concentration measurement. Tartu, 2007, 112 p.
68. **Aime Lust.** Charge state of dopants and ordered clusters formation in CaF_2:Mn and CaF_2:Eu luminophors. Tartu, 2007, 100 p.
69. **Iiris Kahn**. Quantitative Structure-Activity Relationships of environmentally relevant properties. Tartu, 2007, 98 p.
70. **Mari Reinik.** Nitrates, nitrites, N-nitrosamines and polycyclic aromatic hydrocarbons in food: analytical methods, occurrence and dietary intake. Tartu, 2007, 172 p.
71. **Heili Kasuk.** Thermodynamic parameters and adsorption kinetics of organic compounds forming the compact adsorption layer at Bi single crystal electrodes. Tartu, 2007, 212 p.
72. **Erki Enkvist.** Synthesis of adenosine-peptide conjugates for biological applications. Tartu, 2007, 114 p.
73. **Svetoslav Hristov Slavov**. Biomedical applications of the QSAR approach. Tartu, 2007, 146 p.
74. **Eneli Härk.** Electroreduction of complex cations on electrochemically polished Bi(*hkl*) single crystal electrodes. Tartu, 2008, 158 p.
75. **Priit Möller.** Electrochemical characteristics of some cathodes for medium temperature solid oxide fuel cells, synthesized by solid state reaction technique. Tartu, 2008, 90 p.
76. **Signe Viggor.** Impact of biochemical parameters of genetically different pseudomonads at the degradation of phenolic compounds. Tartu, 2008, 122 p.
77. **Ave Sarapuu.** Electrochemical reduction of oxygen on quinone-modified carbon electrodes and on thin films of platinum and gold. Tartu, 2008, 134 p.
78. **Agnes Kütt.** Studies of acid-base equilibria in non-aqueous media. Tartu, 2008, 198 p.

79. **Rouvim Kadis.** Evaluation of measurement uncertainty in analytical chemistry: related concepts and some points of misinterpretation. Tartu, 2008, 118 p.
80. **Valter Reedo.** Elaboration of IVB group metal oxide structures and their possible applications. Tartu, 2008, 98 p.
81. **Aleksei Kuznetsov.** Allosteric effects in reactions catalyzed by the cAMP-dependent protein kinase catalytic subunit. Tartu, 2009, 133 p.
82. **Aleksei Bredihhin.** Use of mono- and polyanions in the synthesis of multisubstituted hydrazine derivatives. Tartu, 2009, 105 p.
83. **Anu Ploom.** Quantitative structure-reactivity analysis in organosilicon chemistry. Tartu, 2009, 99 p.
84. **Argo Vonk.** Determination of adenosine A_{2A}- and dopamine D_1 receptor-specific modulation of adenylate cyclase activity in rat striatum. Tartu, 2009, 129 p.
85. **Indrek Kivi.** Synthesis and electrochemical characterization of porous cathode materials for intermediate temperature solid oxide fuel cells. Tartu, 2009, 177 p.
86. **Jaanus Eskusson.** Synthesis and characterisation of diamond-like carbon thin films prepared by pulsed laser deposition method. Tartu, 2009, 117 p.
87. **Marko Lätt.** Carbide derived microporous carbon and electrical double layer capacitors. Tartu, 2009, 107 p.
88. **Vladimir Stepanov.** Slow conformational changes in dopamine transporter interaction with its ligands. Tartu, 2009, 103 p.
89. **Aleksander Trummal.** Computational Study of Structural and Solvent Effects on Acidities of Some Brønsted Acids. Tartu, 2009, 103 p.
90. **Eerold Vellemäe.** Applications of mischmetal in organic synthesis. Tartu, 2009, 93 p.
91. **Sven Parkel.** Ligand binding to 5-HT_{1A} receptors and its regulation by Mg^{2+} and Mn^{2+}. Tartu, 2010, 99 p.
92. **Signe Vahur.** Expanding the possibilities of ATR-FT-IR spectroscopy in determination of inorganic pigments. Tartu, 2010, 184 p.
93. **Tavo Romann**. Preparation and surface modification of bismuth thin film, porous, and microelectrodes. Tartu, 2010, 155 p.
94. **Nadežda Aleksejeva.** Electrocatalytic reduction of oxygen on carbon nanotube-based nanocomposite materials. Tartu, 2010, 147 p.
95. **Marko Kullapere.** Electrochemical properties of glassy carbon, nickel and gold electrodes modified with aryl groups. Tartu, 2010, 233 p.
96. **Liis Siinor.** Adsorption kinetics of ions at Bi single crystal planes from aqueous electrolyte solutions and room-temperature ionic liquids. Tartu, 2010, 101 p.
97. **Angela Vaasa.** Development of fluorescence-based kinetic and binding assays for characterization of protein kinases and their inhibitors. Tartu 2010, 101 p.

98. **Indrek Tulp.** Multivariate analysis of chemical and biological properties. Tartu 2010, 105 p.
99. **Aare Selberg.** Evaluation of environmental quality in Northern Estonia by the analysis of leachate. Tartu 2010, 117 p.
100. **Darja Lavõgina.** Development of protein kinase inhibitors based on adenosine analogue-oligoarginine conjugates. Tartu 2010, 248 p.
101. **Laura Herm.** Biochemistry of dopamine D_2 receptors and its association with motivated behaviour. Tartu 2010, 156 p.
102. **Terje Raudsepp.** Influence of dopant anions on the electrochemical properties of polypyrrole films. Tartu 2010, 112 p.
103. **Margus Marandi.** Electroformation of Polypyrrole Films: *In-situ* AFM and STM Study. Tartu 2011, 116 p.
104. **Kairi Kivirand.** Diamine oxidase-based biosensors: construction and working principles. Tartu, 2011, 140 p.
105. **Anneli Kruve.** Matrix effects in liquid-chromatography electrospray mass-spectrometry. Tartu, 2011, 156 p.
106. **Gary Urb.** Assessment of environmental impact of oil shale fly ash from PF and CFB combustion. Tartu, 2011, 108 p.
107. **Nikita Oskolkov.** A novel strategy for peptide-mediated cellular delivery and induction of endosomal escape. Tartu, 2011, 106 p.
108. **Dana Martin.** The QSPR/QSAR approach for the prediction of properties of fullerene derivatives. Tartu, 2011, 98 p.
109. **Säde Viirlaid.** Novel glutathione analogues and their antioxidant activity. Tartu, 2011, 106 p.
110. **Ülis Sõukand.** Simultaneous adsorption of Cd^{2+}, Ni^{2+}, and Pb^{2+} on peat. Tartu, 2011, 124 p.
111. **Lauri Lipping.** The acidity of strong and superstrong Brønsted acids, an outreach for the "limits of growth": a quantum chemical study. Tartu, 2011, 124 p.
112. **Heisi Kurig.** Electrical double-layer capacitors based on ionic liquids as electrolytes. Tartu, 2011, 146 p.
113. **Marje Kasari.** Bisubstrate luminescent probes, optical sensors and affinity adsorbents for measurement of active protein kinases in biological samples. Tartu, 2012, 126 p.
114. **Kalev Takkis.** Virtual screening of chemical databases for bioactive molecules. Tartu, 2012, 122 p.
115. **Ksenija Kisseljova**. Synthesis of aza-β^3-amino acid containing peptides and kinetic study of their phosphorylation by protein kinase A. Tartu, 2012, 104 p.
116. **Riin Rebane.** Advanced method development strategy for derivatization LC/ESI/MS. Tartu, 2012, 184 p.

117. **Vladislav Ivaništšev.** Double layer structure and adsorption kinetics of ions at metal electrodes in room temperature ionic liquids. Tartu, 2012, 128 p.
118. **Irja Helm.** High accuracy gravimetric Winkler method for determination of dissolved oxygen. Tartu, 2012, 139 p.
119. **Karin Kipper.** Fluoroalcohols as Components of LC-ESI-MS Eluents: Usage and Applications. Tartu, 2012, 164 p.
120. **Arno Ratas.** Energy storage and transfer in dosimetric luminescent materials. Tartu, 2012, 163 p.
121. **Reet Reinart-Okugbeni**. Assay systems for characterisation of subtype-selective binding and functional activity of ligands on dopamine receptors. Tartu, 2012, 159 p.
122. **Lauri Sikk.** Computational study of the Sonogashira cross-coupling reaction. Tartu, 2012, 81 p.
123. **Karita Raudkivi.** Neurochemical studies on inter-individual differences in affect-related behaviour of the laboratory rat. Tartu, 2012, 161 p.
124. **Indrek Saar.** Design of GalR2 subtype specific ligands: their role in depression-like behavior and feeding regulation. Tartu, 2013, 126 p.
125. **Ann Laheäär.** Electrochemical characterization of alkali metal salt based non-aqueous electrolytes for supercapacitors. Tartu, 2013, 127 p.